Peer reviewed version of the manuscript published in final form at Langmuir (2021)

Design of lipid-based nanocarriers via cation modulation of ethanol-interdigitated lipid membranes

Valeria Nele[1], Margaret N. Holme[1,2], M. Harunur Rashid[3,4], Hanna M. G. Barriga[2], Tu C. Le[3], Michael R. Thomas[1,6], James J. Doutch[5], Irene Yarovsky[3]*, Molly M. Stevens[1,2]**

[1]Department of Materials, Department of Bioengineering and Institute of Biomedical Engineering Imperial College London, London, SW7 2AZ, UK

[2]Department of Medical Biochemistry and Biophysics, Karolinska Institutet, SE-171 77 Stockholm, Sweden

[3]School of Engineering, RMIT University, Melbourne, Victoria, 3001, Australia

[4]Department of Mathematics and Physics, North South University, Bashundhara, Dhaka, 1229, Bangladesh

[5]ISIS Neutron and Muon Source, STFC, Rutherford Appleton Laboratory, Didcot, OX11 ODE, UK

[6]London Centre for Nanotechnology and Department of Biochemical Engineering, University College London, 17−19 Gordon Street, London, WC1H 0AH, UK

Correspondence to:

* Email: irene.yarovsky@rmit.edu.au ** Email: m.stevens@imperial.ac.uk

ABSTRACT

Short-chain alcohols (*i.e.*, ethanol) can induce membrane interdigitation in saturated-chain phosphatidylcholines (PCs). In this process, the alcohol molecules intercalate between the phosphate heads, increasing lateral separation and favoring hydrophobic interactions between opposing acyl chains, that interpenetrate forming an interdigitated phase. Unravelling the mechanisms underlying the interactions between ethanol and model lipid membranes has implications for cell biology, biochemistry, and for the formulation of lipid-based nanocarriers. However, investigations of ethanol-lipid membrane systems have been carried out in deionized water, which limits their applicability. Here, by using a combination of small- and wide-angle X-ray scattering, small-angle neutron scattering and all-atom molecular dynamics simulations, we analyzed the effect of varying $CaCl_2$ and NaCl concentrations on ethanol-induced interdigitation. We observed that while ethanol addition leads to the interdigitation of bulk phase DPPC bilayers in the presence of $CaCl_2$ and NaCl regardless of the salt concentration, the ethanol-induced interdigitation of vesicular DPPC depends on the choice of cation and its concentration. These findings unravel a key role for cations in the ethanol-induced interdigitation of lipid membranes in either bulk phase or vesicular form.

Keywords: phospholipids, vesicles, nano-carriers, membrane interdigitation, X-ray scattering, neutron scattering, all-atom molecular dynamics simulations.

Phospholipids undergo reversible gel to liquid crystalline (L_α) phase transitions across a wide range of temperatures and pressures. Their phase behaviour has important implications for many membrane properties, such as permeability, shape, and stiffness.[1] The gel phase often presents a certain degree of polymorphism: in addition to the most prominent gel phases L_β (untilted chains) and $L_{\beta'}$ (tilted chains), for some lipids it is possible to identify a sub-gel phase (L_c), a ripple gel phase ($P_{\beta'}$), and an interdigitated gel phase ($L_{\beta I}$).[2] In the $L_{\beta I}$ phase the lateral separation between the phospholipid headgroups increases and the chains of the two bilayer leaflets interdigitate, with a reduction of the bilayer thickness. Phospholipid molecules can exhibit a certain degree of chain asymmetry: the two acyl chains can differ by their length or degree of saturation, or both. Chain length asymmetry can be quantified by the chain inequivalence parameter (*i.e.* the ratio between the difference in the chain lengths and the length of the longest chain) and can give rise to partial or mixed interdigitation.[3]

The chemical structure of phospholipids has a profound effect on the preferred bilayer configuration in the gel phase. As an example, ester-linked diacyl-phosphatidylcholines with chains of at least 22 carbon atoms long spontaneously exhibit the $L_{\beta I}$ phase as a result of the stronger hydrophobic interactions between the long acyl chains.[4] Phosphatidylcholines (PCs) with an ether bond instead of the ester linkage exhibit the $L_{\beta I}$ phase regardless of the chain length, as a consequence of the weaker attractive forces between their headgroups.[5] The tail position on the glycerol backbone is also important: it has been shown that the amide linkage in the 1,3 position leads to interdigitated bilayers while the same linkage in the 1,2 position gives a non-interdigitated bilayer.[6] Repulsion between charged headgroups in cationic lipids leads to bilayer interdigitation and may have implications for vesicle fusion.[7,8] Replacing the terminal carbon in one of the two acyl chains with fluorine also favors an interdigitated configuration.[9] Alternatively, bilayer interdigitation can be induced by physical or chemical cues. High pressure has been shown to induce bilayer interdigitation in saturated, ester-linked phosphocholines with a carbon number between 14 and 21.[10] The addition of small molecules such as anesthetics, acetonitrile and short-chain alcohols induces interdigitation in PC bilayers upon insertion of these molecules between the phospholipid headgroups.[11–13]

Understanding the interactions between short-chain alcohols, such as ethanol, and model lipid membranes has implications for cell biology, as ethanol exposure can deeply affect the functionality of cells,[14] and biochemistry, as the bilayer composition has been shown to affect the ethanol tolerance of yeasts used for alcoholic fermentation.[15] Furthermore, ethanol is a key component of ethosomes, which exhibit enhanced skin penetration over other lipid-based nanocarriers,[16] and is used for the microfluidic production of liposomes.[17] Ethanol-induced interdigitation of diacyl-PC bilayers has also been exploited to introduce a liposome formulation method, namely the interdigitation-fusion vesicle method, that yields large unilamellar vesicles with high entrapped aqueous volumes, as

opposed to *e.g.* the lipid film hydration method, which yields large multilamellar vesicles.[18] In the interdigitation-fusion vesicle method ethanol is added to a small unilamellar vesicle (SUV) suspension below the lipid transition temperature (T_m), causing vesicle fusion and rupture, together with bilayer interdigitation (**Figure 1**). This phenomenon is accompanied by a *sol-gel* transition of the vesicle suspension. Raising the temperature above the T_m allows the refolding of the interdigitated bilayers into large unilamellar vesicles. This method has been exploited to formulate vesosomes: large, multicompartment unilamellar vesicles entrapping SUVs or metal-based nanoparticles.[19–21]
Given the relevance of ethanol-lipid membrane interactions, a variety of techniques, including nuclear magnetic resonance (NMR), all-atom molecular dynamics (MD) simulations, fluorescence-based assays, and X-ray diffraction measurements have been used to study the effect of ethanol on lipid bilayers.[22–25] In order to induce bilayer interdigitation, ethanol needs to replace water molecules at the lipid-water interface, altering the magnitude of the hydration forces responsible for inter-bilayer repulsion.[26,27] The water layer coordinated to the lipid bilayer can also be modified by the presence of cations that bind to the polar headgroups of the phospholipid molecules.[28] In particular, adsorption of ions on neutral lipid bilayers leads to the accumulation of electrostatic charge; this phenomenon generally follows the Hofmeister series, and larger ions give higher measured electrostatic potentials.[29] Ion-specific bilayer swelling is observed with increasing ion concentration, depending on the solvation properties of the ion.[29,30]

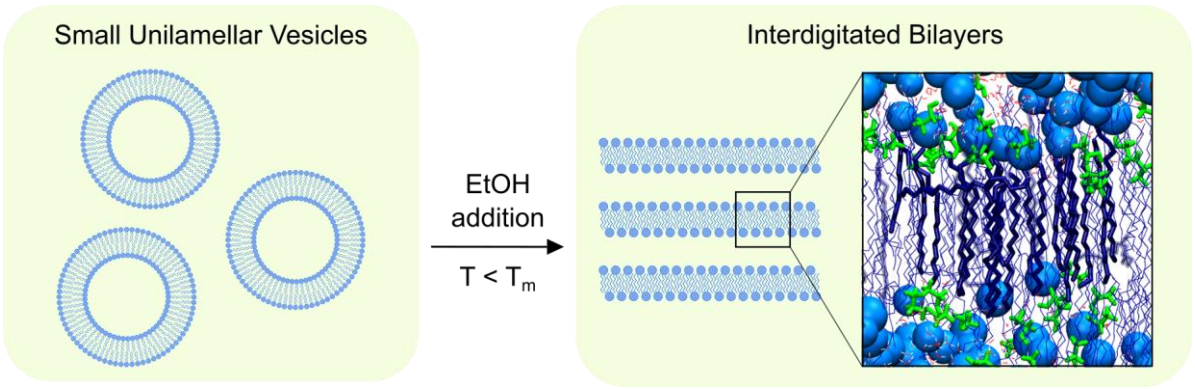

Figure 1. Schematic of ethanol-induced membrane interdigitation. The addition of ethanol (showed in green) to small unilamellar vesicles below the lipid T_m leads to the formation of bilayer stacks, which exhibit an interdigitated membrane.

Despite numerous investigations on the interactions between ethanol and PC bilayers in the context of bilayer interdigitation, little is known on the role of cations, in particular Ca^{2+} and Na^{+}. Here, we used small- and wide-angle X-ray scattering (SAXS and WAXS), small-angle neutron scattering (SANS), and all-atom MD simulations to elucidate the nature of the complex interactions between calcium and sodium ions, ethanol, and PC membranes.

SAXS/WAXS and SANS are powerful techniques that provide structural information on phospholipidic ensembles. SAXS and WAXS are particularly suited for bulk phase measurements, offering excellent Bragg peak resolution and insights into the lipid chain packing. Vesicle samples containing multiple lipid bilayers can also be measured with X-ray scattering but the signal to noise ratio is lower than for bulk samples due to the lower number of repeat units. SANS is especially useful in this sense: it exploits the neutron contrast between deuterium and hydrogen, which allows high signal to noise ratio from vesicle samples at low concentrations from protonated samples in deuterated solvents. Quantitative information on the membrane bilayer thickness, vesicle diameter and overall morphology can be obtained by fitting of SANS data. We complemented the information obtained from X-ray and neutron scattering of bulk phase lipid samples with all-atom MD simulations, which unraveled the interactions at play between the different components on atomistic length scales. All-atom MD simulations have been extensively used to study many properties of biological membranes. These include the structure of bilayers comprising a single lipid or lipid mixtures,[31,32] the effect of ions on lipid arrangement and mixing,[33,34] and the interactions of membrane proteins[35,36] and enzymes[37] with the bilayer. The results obtained here uncover the role of calcium and sodium ions in ethanol-induced interdigitation of bulk phase and vesicular DPPC, with broad implications for cell biology and biochemistry, as well as for the formulation of lipid-based nanocarriers.

RESULTS AND DISCUSSION

Effect of sodium ions on DPPC – ethanol systems

To probe the effect of sodium ions on ethanol-induced interdigitation of DPPC bilayers, we first carried out SAXS and WAXS measurements on bulk DPPC systems equilibrated with 4 M ethanol and aqueous solutions of varying NaCl concentrations. DPPC has been previously shown to exhibit interdigitation at this ethanol concentration in water.[25] Measurements were carried out at 25 °C; at this temperature, DPPC bilayers in the absence of ethanol are in the $L_{\beta'}$ phase.[38] The measured X-ray scattering data are shown in **Figure 2**.

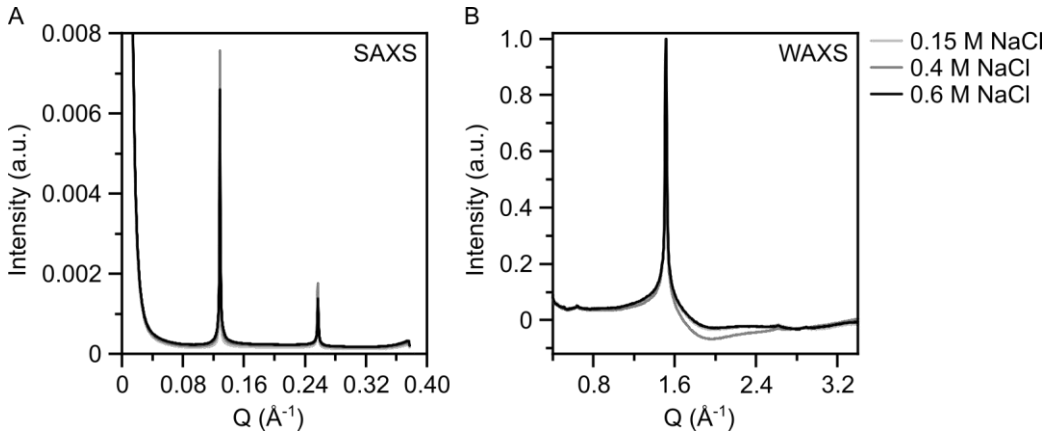

Figure 2. SAXS (A) and WAXS (B) measurements of DPPC bulk mixtures equilibrated with 4 M ethanol and aqueous solutions containing 0.15, 0.4, and 0.6 M NaCl. Measurements were carried out at 25 °C.

We observed sharp lamellar reflections in the small-angle region for all the NaCl concentrations studied. To obtain the corresponding d-spacings, we fitted the SAXS data using AXcess.[39] The d-spacing (or lamellar repeat distance) is the sum of the bilayer thickness and the coordinated water layer. In this case, the DPPC bulk mixtures were all characterised by a d-spacing of 48.9 - 49.0 Å (**Table S1**). This value is indicative of bilayer interdigitation and is in good agreement with previous literature.[40] For comparison, the d-spacing of DPPC in water in the gel phase $L_{\beta'}$ is 64 Å.[41] Analysis of the WAXS data provided insights into the lipid packing within the interdigitated bilayer. In particular, the chain-chain lattice distances could be estimated. Here, the samples exhibited a sharp reflection at Q = 1.51 $Å^{-1}$, which corresponds to a d-spacing = 4.15 Å, indicating a hexagonal packing of the hydrocarbon chains.[42] Overall, the SAXS and WAXS measurements of bulk phase DPPC showed no effect of NaCl concentration on ethanol-induced bilayer interdigitation under these conditions.

Small unilamellar vesicles have been shown to form interdigitated bilayer sheets upon addition of ethanol above a threshold concentration. Komatsu *et al.* proposed a mechanism for ethanol-induced vesicle aggregation, fusion, and bilayer interdigitation.[43] According to them, the ethanol acts by displacing the water molecules coordinated to the surface of the vesicles, which reduces the hydration forces between two adjacent bilayers and initiates aggregation. When the two bilayers come into contact, they start to interdigitate, which leads to stabilization of the adhering bilayers and eventually to bilayer joining and fission.[43] In order to elucidate the role of sodium in ethanol-induced interdigitation of small unilamellar vesicles, we performed the same set of X-ray scattering measurements on DPPC vesicles hydrated with selected concentrations of aqueous NaCl (0.15, 0.4, and 0.6 M). The vesicles were extruded 35 times through 100 nm and 50 nm pore-sized membranes prior to the addition of 4 M ethanol. The SAXS and WAXS data are shown in **Figure S1**. Compared to the bulk mixtures, the SAXS data of the vesicle samples exhibited reduced scattering intensity

and/or peak broadening, which suggests that the vesicle samples exhibited a broader range of d-spacings compared to the bulk samples. Importantly, the extracted d-spacings and the behavior of bulk and vesicle samples in relation to NaCl concentration and ethanol interdigitation were comparable. It is worth mentioning that these vesicles possess some degree of multilamellarity;[44] multilamellar vesicles have fewer repeat units compared to bulk phase mixtures and may exhibit a range of d-spacings, which results in reduced peak intensities and broader peaks compared to the lamellar stacks.[45] Nevertheless, the d-spacings for the vesicle samples could still be obtained by fitting the SAXS data with AXcess (**Table S2**). Also in this case, we obtained d-spacings around 49 Å, which suggest interdigitated bilayers. The errors of the fitted d-spacings are higher compared to the bulk samples due to the lower scattering intensity and the presence of broad peaks in the vesicle samples. In the wide-angle region, the vesicle samples had a similar profile to the bulk phase samples, exhibiting a sharp peak at Q = 1.51 $Å^{-1}$, which corresponds to a reflection at 4.15 Å. By using complementary small-angle neutron scattering measurements, the thickness of the water layer can be estimated by using suitable fitting models. To this end, we carried out SANS measurements on DPPC vesicles extruded through 100 nm and then 50 nm pore-sized membranes. We then added partially deuterated ethanol (CH_3CH_2OD) to a final concentration of 4 M to induce interdigitation at 25 °C. Partially deuterated ethanol was preferred to non-deuterated ethanol to lower the total concentration of ^1H in the sample, which reduced the incoherent scattering at high Q and avoided variations in the background scattering due to ethanol proton exchange in a deuterated environment. The neutron scattering data were first fitted with a Broad Peak model to determine the d-spacing and are shown in **Figure 3**. This model combines a Lorentzian-peak function and a power law decay (for more details, see Supporting Information). The fitting parameters are reported in **Table S3**. The fitted Porod exponent exhibited values between 3.00 and 3.23, which are typical of rough interfaces. The Lorentz screening length lies between 47.19 Å (0.4 M NaCl) and 53.87 Å (0.6 M NaCl). This parameter is the inverse of the Bragg peak width; its increase is due to the sharpening of the peak in the presence of salt. The d-spacing was 52.36 Å for all the conditions, only 3.36 Å higher than the fitted d-spacing from the X-ray scattering measurements (~ 49 Å). The reduced scattering intensity for the 0.6 M NaCl sample may be due to vesicle aggregation and precipitation upon ethanol addition, as shown by DLS measurements (**Figure 3E**).

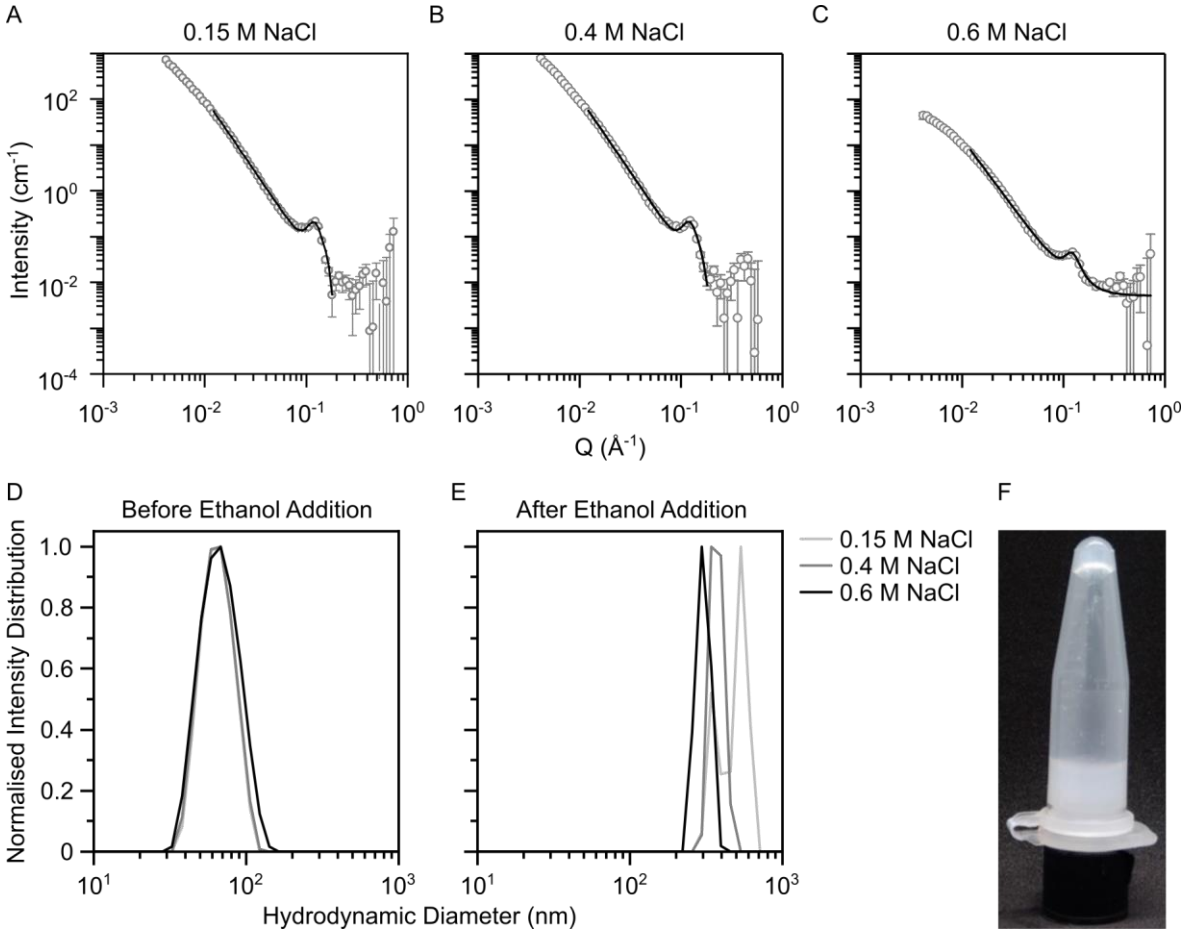

Figure 3. Neutron scattering data of DPPC vesicles containing 0.15 M (A), 0.4 M (B), and 0.6 M (C) NaCl and equilibrated with 4 M CH_3CH_2OD at 25 °C. Prior to CH_3CH_2OD addition, the vesicles were extruded 35 times through 100 nm and then 50 nm pore-sized membranes. Points with errors represent measured data while lines represent fits obtained with a Broad Peak model. Data are plotted on a log-log scale. Dynamic light scattering measurements of DPPC vesicles containing aqueous solutions of 0.15, 0.4, and 0.6 M NaCl before (D) and after (E) addition of ethanol to a final concentration of 4 M at 25 °C. (F) Representative picture of DPPC vesicles upon ethanol addition showing that the vesicle suspension remains liquid.

We also used a Multilayer Vesicle model to fit the portion of the curves between 0.028 and 0.195 $Å^{-1}$ to determine the bilayer thickness and calculate the water layer thickness. This model provides structural information on multilamellar vesicle systems (for more details, see Supporting Information). The neutron scattering data and relative fits are shown in **Figure S2** while the fitting parameters are reported in **Table S4**. The best-fit bilayer thickness was 37 Å for all the NaCl concentrations studied, which seems to be intermediate between the bilayer thickness of interdigitated DPPC bilayers in the presence of water and 1.7 M ethanol (31 Å)[46] and the bilayer thickness of gel phase DPPC in phosphate buffered saline (*ca.* 45 Å).[44] The increase in the bilayer thickness we observed for DPPC-ethanol systems may be due to the presence of salt; for example, bilayer thickening has been previously reported for fluid phase POPC in the presence of NaCl at

concentrations higher than 1 M.[47] However, to the best of our knowledge, the effect of NaCl on the thickness of DPPC bilayers has yet to be reported. Alternatively, the bilayer thickness observed for the DPPC-ethanol-NaCl systems may be indicative of a partially interdigitated system comprising either two vesicle populations, one with interdigitated membranes and one with bilayers in the $L_{\beta'}$ phase, or one vesicle population where interdigitated membrane domains coexist with $L_{\beta'}$ domains. The existence of interdigitated domains within DPPC bilayers incubated with varying ethanol concentrations has been previously probed *via* atomic force microscopy.[48] In both cases, this would result in a reduction in the average bilayer thickness in neutron scattering measurements compared to gel phase DPPC bilayers. The best-fit water layer thickness was also reduced for the DPPC-ethanol-NaCl systems, possibly because of the ethanol dehydration effect. Ethanol possesses hydrogen bonding ability and is able to displace water at the bilayer interface;[49] this results in an increase in the lipid area and a reduction in the bilayer thickness, which eventually leads to interdigitation.[25] The number of shells estimated by the Multilayer Vesicle model was 5; our group has previously shown that a small fraction (approximately 10 vol%) of DPPC vesicles are bilamellar after extrusion through a 100 nm pore-sized membrane.[44] Here, the vesicles were also extruded through a 50 nm membrane, which could have further reduced the fraction of non-unilamellar ensembles, as previously shown for POPC vesicles.[50] The presence of multilamellar vesicles upon ethanol addition may be due to aggregation phenomena. The absence of a Guinier region, *i.e.*, a dip in the scattering curves at low Q, which is representative of the core radius, suggests that the system is either highly polydisperse or it comprises vesicles with radii of 100s to 1000s of nm, which exhibit a Guinier region at Q values outside of the Q range probed in this instrument configuration. Therefore, estimates of the core radii are not reliable in this context. To gain further insight into the effect of ethanol on SUV suspensions, we performed dynamic light scattering measurements of DPPC vesicles in 0.15, 0.4, and 0.6 M NaCl before and after ethanol addition (**Figure 3D,E**). Vesicles were extruded through 100 and then 50 nm pore-sized membranes and exhibited hydrodynamic diameters of approximately 63 nm and low polydispersity in absence of ethanol. We observed substantial changes in the hydrodynamic diameter of the vesicles upon ethanol addition, which was reflected in large hydrodynamic diameters and high polydispersities and may be indicative of vesicle aggregation (for exact figures, see **Table S5**). Furthermore, the vesicle suspension remained liquid and an increase of turbidity was observed (**Figure 3F**), which suggests the presence of large scattering bodies at these length scales. The DLS measurements corroborated the neutron scattering data and confirmed that in the presence of varying concentration of NaCl, ethanol induces changes in small unilamellar vesicle populations, which could be due to aggregation phenomena.

Effect of calcium ions on DPPC – ethanol systems

Calcium ions have been shown to bind more strongly to phosphatidylcholine bilayers compared to sodium ions: the intrinsic binding constants are 40 M^{-1} (Ca^{2+}) and 0.15 M^{-1} (Na^{+}).[51] These two ions have similar atomic radii (0.99 and 0.97 Å) but the charge squared-radius ratio, which measures the ionic solvation interaction, is four times higher for calcium compared to sodium.[52] As a result, calcium ions impact the behavior of PC bilayers, including alterations in the lipid phase transition, partial dehydration and conformational changes.[53] The ethanol-induced interdigitation of DPPC bilayers was studied in the presence of varying concentrations of $CaCl_2$. In analogy with the NaCl series, we first carried out SAXS and WAXS measurements on DPPC bulk mixtures equilibrated with 0.15, 0.4, or 0.6 M $CaCl_2$ and 4 M ethanol. The scattering data are shown in **Figure 4** while the fitted d-spacings for the mixtures containing 0.4 and 0.6 M $CaCl_2$ are reported in **Table S6**.

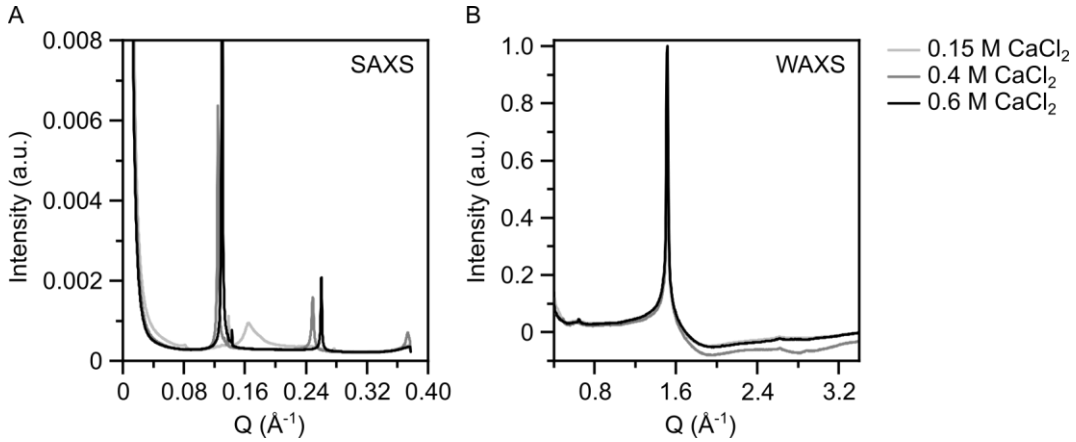

Figure 4. SAXS (A) and WAXS (B) measurements of DPPC bulk mixtures equilibrated with 4 M ethanol and aqueous solutions containing 0.15, 0.4, and 0.6 M $CaCl_2$. Measurements were carried out at 25 °C.

It was not possible to obtain a d spacing for 0.15 M $CaCl_2$ because of potential phase separation within the sample. As opposed to the NaCl series, the SAXS data showed broad peaks at 0.15 M $CaCl_2$, while sharp lamellar reflections were observed for 0.4 and 0.6 M $CaCl_2$, with d-spacings of 50.54 and 48.36 Å. These values suggest the existence of interdigitated bilayers. DPPC bilayers have been previously shown to exhibit broad peaks between 0.005 and 0.05 M $CaCl_2$ and sharp lamellar reflections above 0.5 M $CaCl_2$ due to concentration-dependent charge screening effects which alter the magnitude of inter-bilayer forces.[54,55] The wide-angle region showed an identical pattern to the NaCl series, with a sharp reflection at Q = 1.51 $Å^{-1}$, which corresponds to d = 4.15 Å, indicative of hexagonal packing of the hydrocarbon chains. In analogy to the NaCl series, we performed SAXS and WAXS measurements on DPPC vesicles hydrated with selected concentrations of aqueous $CaCl_2$

(0.15, 0.4, and 0.6 M). The vesicles were extruded 35 times through 100 nm and then 50 nm pore-sized membranes prior to the addition of 4 M ethanol at 25 °C. The SAXS and WAXS data are shown in **Figure S3**. The scattered intensity of the vesicles was lower than the bulk samples, and the 0.15 M $CaCl_2$ sample exhibited a single broad peak, as opposed to the 0.4 and 0.6 M $CaCl_2$. The fitted d-spacings for the vesicle samples in 0.4 and 0.6 M $CaCl_2$ are shown in **Table S7**. The error in the best-fit d-spacing is higher compared to the bulk phase samples due to peak broadening in the vesicle X-ray scattering data. The 0.15 M $CaCl_2$ scattering data could not be fitted with the AXcess software due to the extent of peak broadening, which suggests the presence of a wide range of spacings within the sample. However, we calculated an indicative lattice parameter by taking the position of the peak maximum and obtained a value of 36.84 Å which is in good agreement with the broad peak observed in the bulk SAXS data. We carried out small-angle neutron scattering measurements on DPPC vesicles to determine the bilayer and the water layer thicknesses. In this case, the DPPC vesicles were prepared with solutions of varying $CaCl_2$ concentrations in deuterated water and extruded 35 times through 100 nm and then 50 nm pore-sized membranes. Partially deuterated ethanol (CH_3CH_2OD) to a final concentration of 4 M was then added to induce interdigitation. The neutron scattering data of the 0.15 M $CaCl_2$ sample could be fitted with a simple Lamellar model and are shown in **Figure 5A**. We obtained a best-fit bilayer thickness of 25.12 ± 0.34 Å, suggesting bilayer interdigitation. Prior to ethanol addition, the vesicles exhibited hydrodynamic diameters of 59 nm and polydispersity of 0.051, as measured by dynamic light scattering (**Figure 5B**). Ethanol addition below the lipid T_m induced vesicle rupture and fusion in interdigitated lamellar stacks, which resulted in a *sol-gel* transition of the vesicle suspension (**Figure 5C**).

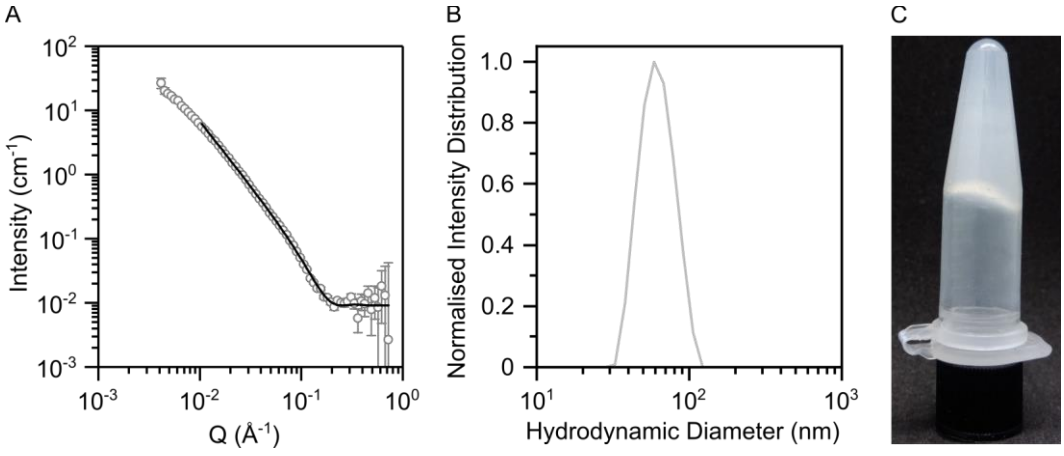

Figure 5. (A) Neutron scattering data of DPPC vesicles containing 0.15 M $CaCl_2$ and equilibrated with 4 M CH_3CH_2OD at 25 °C. Prior to CH_3CH_2OD addition, the vesicles were extruded 35 times through 100 nm and then 50 nm pore-sized membranes. Points with errors represent measured data while lines represent fits obtained with a Lamellar model. Data are plotted on a log-log scale. (B) Dynamic light scattering measurements of DPPC vesicles containing aqueous solutions of 0.15 M

$CaCl_2$ prior to ethanol addition to a final concentration of 4 M. (C) Representative picture of DPPC vesicles upon ethanol addition showing that the vesicle suspension turns into a gel.

Neutron scattering data of samples containing 0.4 and 0.6 M $CaCl_2$ bore similarities to the samples prepared in aqueous solutions of NaCl. We first used a Broad Peak model to determine the d-spacings, as shown in **Figure 6A,B** and **Table S8**. The best-fit Porod exponents were 2.97 and 3.78 for the samples in 0.4 M and 0.6 M $CaCl_2$, respectively. The difference in the Porod exponents is reflected in the slopes of the relative neutron scattering curves; in both cases, these values are typical of rough interfaces. The Lorentz screening length increased when increasing the $CaCl_2$ concentration from 0.4 to 0.6 M. The d-spacing was reduced from 52.36 Å to 48.33 Å and was in good agreement with the fitted d-spacing from the X-ray scattering measurements.

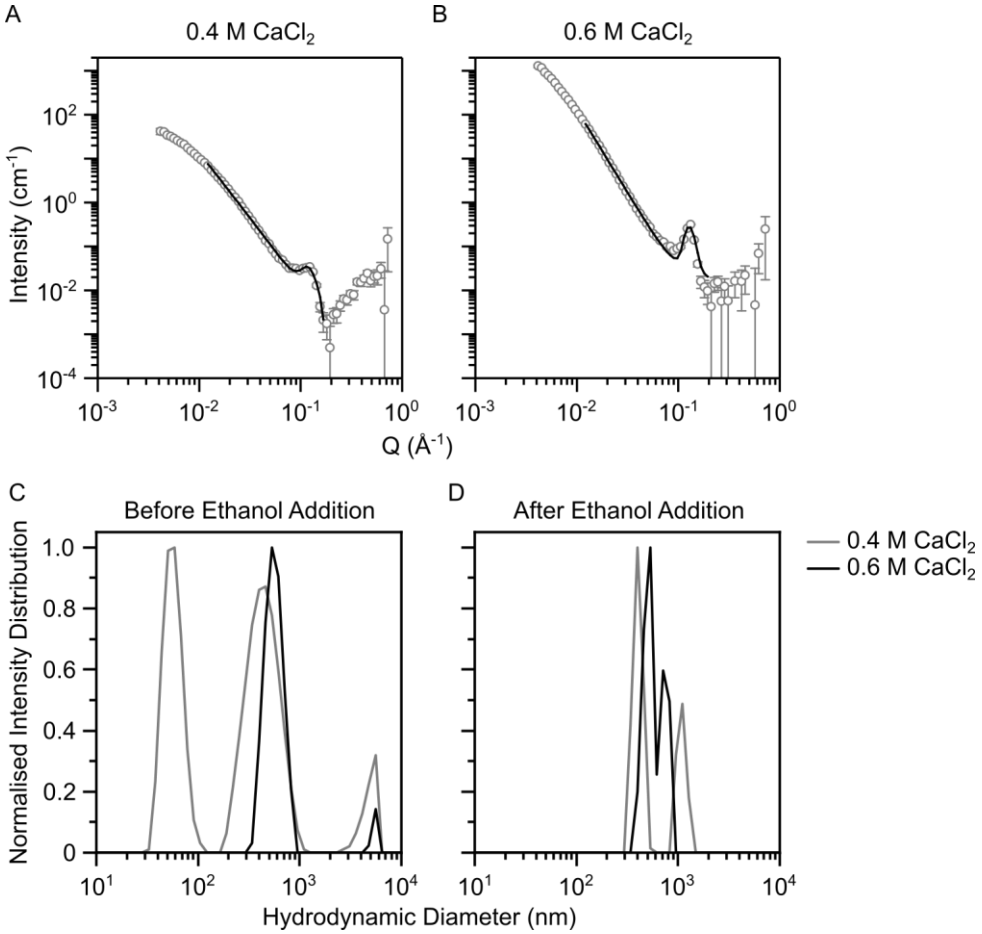

Figure 6. Neutron scattering data of DPPC vesicles containing 0.4 M (A) and 0.6 M (B) $CaCl_2$ and equilibrated with 4 M CH_3CH_2OD at 25 °C. The vesicles were extruded 35 times through a 100 nm and then 50 nm pore-sized membranes before adding an appropriate volume of CH_3CH_2OD. Points with errors represent measured data while lines represent fits obtained with a Broad Peak model. Data are plotted on a log-log scale. Dynamic light scattering measurements of DPPC vesicles containing

aqueous solutions of 0.4 and 0.6 M $CaCl_2$ before (C) and after (D) addition of ethanol to a final concentration of 4 M at 25 °C.

We then used a Multilayer Vesicle model to fit the portion of the curves between 0.028 and 0.211 $Å^{-1}$ to determine the bilayer thickness and calculate the water layer thickness for the 0.6 M $CaCl_2$ sample. The neutron scattering data and relative fits are shown in **Figure S4** while the fitting parameters are reported in **Table S9**. Also in this case, we obtained a bilayer thickness that is 6 Å higher than the thickness of interdigitated DPPC bilayers equilibrated with water and 1.7 M ethanol.[46] At the same time, this value is smaller compared to the thickness of DPPC bilayers in the $L_{\beta'}$ phase.[44] The best-fit bilayer thickness could be indicative of a partially interdigitated system, which could comprise one vesicle population with interdigitated membrane domains coexisting with $L_{\beta'}$ domains. The best-fit water layer thickness was 12 Å, in analogy to the NaCl series. The number of shells estimated by the Multilayer Vesicle model was 15 for the 0.6 M $CaCl_2$ sample; this could be due to the presence of lamellar stacks. Dynamic light scattering measurements for DPPC vesicles in 0.4 and 0.6 M $CaCl_2$ before and after ethanol addition showed substantial changes in the hydrodynamic diameter for both the $CaCl_2$ concentrations explored (**Figure 6C,D** and **Table S10**). In both cases, the vesicle suspension remained liquid upon incubation with ethanol. Komatsu *et al.* have previously shown that DPPC small unilamellar vesicles incubated with ethanol above 1 M undergo a rapid size increase, which could be attributed to vesicle aggregation rather than fusion. Additionally, the aggregation state was related to the onset of bilayer interdigitation as they are both driven by bilayer dehydration.[43] It has been shown that the concentration of ethanol required to induce bilayer interdigitation is dependent on the vesicle size, with smaller unilamellar vesicles of 100-200 nm in diameter requiring higher ethanol concentrations to initiate interdigitation. Importantly, small unilamellar vesicles were shown to fuse in interdigitated lamellar sheets, which exhibited a transition from a liquid to a viscous, gel-like suspension easily detectable by eye,[56] in agreement with our observations for DPPC vesicles incubated with 0.15 M $CaCl_2$ and ethanol.

At all the NaCl concentrations studied, the addition of ethanol was not able to induce vesicle fusion into interdigitated lamellar stacks, as previously reported.[57] Instead, in the presence of NaCl, ethanol may have triggered vesicle aggregation into larger structures (as shown by DLS measurements), and the resulting d-spacing and bilayer thickness were reduced compared to the values found for $L_{\beta'}$ phase bilayers, suggesting the presence of partial membrane interdigitation. In the presence of 0.15 M $CaCl_2$, ethanol was able to induce vesicle fusion in interdigitated lamellar stacks, which was accompanied by a *sol-gel* transition of the vesicle suspension. At higher $CaCl_2$ concentrations, however, we observed a similar behaviour to the NaCl system upon ethanol addition while DLS measurements showed substantial increase in the hydrodynamic diameters before ethanol addition. It is possible that for the fusion in interdigitated lamellar stacks to happen, the vesicles are required to

exhibit high curvature and small diameters. Vesicle fusion into interdigitated lamellar stacks, with the resulting *sol-gel* transition of the vesicle suspension, is crucial for the production of interdigitation-fusion vesicles, which form upon refolding of such lamellar stacks incubated at temperatures above the lipid T_m.[18] In this regard, the presence of fusion-inducing agents, such as calcium ions, is crucial.

All-atom molecular dynamics simulations

In order to gain insights into the interactions between the lipid bilayer, calcium and sodium ions, ethanol, and water at atomistic length scales, we carried out all-atom molecular dynamics simulations in an explicit solvent for a DPPC bilayer consisting of 72 lipid molecules per leaflet equilibrated with 4 M ethanol and aqueous solutions containing either 0.15 or 0.6 M NaCl or $CaCl_2$. After 600 ns of MD simulations, a fraction of the DPPC bilayer in 0.15 M NaCl was interdigitated (**Figure 7A**), whereas only the terminal portion of the lipid chains of the DPPC bilayer were shown to overlap in 0.6 M NaCl (**Figure S5**). Sodium and calcium ion binding has been previously shown to require circa 30 and 100 ns to reach equilibrium conditions in MD simulations, respectively.[58] Hence, the 600 ns simulation can be expected to provide accurate information on the ionic behaviour, as well as atomistic insights into the initial period of the interdigitation process. We found that ethanol interacted with the lipid headgroups for both the NaCl concentrations examined (**Figure 7B,C** and **Figure S5B,C**). DPPC has eight oxygen atoms that can act as hydrogen bond acceptors for ethanol; of these, four are covalently bound to the phosphate atoms, two belong to the glycerol backbone, and two are covalently bound to the carbonyl moiety.[59] We calculated the radial distribution functions (RDFs) for ethanol coordination with the phosphate and the carbonyl oxygens of DPPC molecules (**Figure 7B** and **Figure S5B**) to quantify the nature of this interaction. Here, we present the probability of finding ethanol molecules and carbonyl or phosphate oxygens at a particular distance r. The RDFs showed that ethanol was preferentially bound to the phosphate oxygens at both 0.15 and 0.6 M NaCl (**Figure 7B** and **Figure S5B**) in the region between 2 and 4 Å, in agreement with previous work.[59] For a hydrogen bond to form, the distance between the donor and the acceptor molecules has to be smaller than 2.5 Å.[23] Due to its amphipathic nature, ethanol can penetrate deep within the bilayer; furthermore ethanol molecules tend to localize at the lipid-water interface, as shown by the peak in the number density at 40 Å (**Figure 7F** and **Figure S5F**). This could lead to an increase in lipid area and membrane fluidity, which results in the reduction of both the membrane thickness and the surface tension at the lipid-water interface.[60] We also observed that the sodium ions interacted with the lipid headgroups (**Figure 7D,E** and **Figure S5D,E**), and we calculated RDFs for Na^+ coordination with the phosphate and the carbonyl oxygen of DPPC molecules (**Figure 7D** and **Figure S5D**). For both the NaCl concentrations studied, the RDFs showed a preferential coordination of Na^+ to the carbonyl

oxygens compared to the phosphate oxygens in the region between 2 and 4 Å, in agreement with previous work.[61] Binding of sodium ions to the carbonyl oxygen of phosphocholines results in bilayer compression and a reduced area per lipid headgroup.[58] Furthermore, Na^+ ions penetrated deep in the bilayer to the carbonyl oxygen region, as seen from the number density at a distance of 20 Å from the bilayer center (**Figure 7F,G** and **Figure S5F,G**).

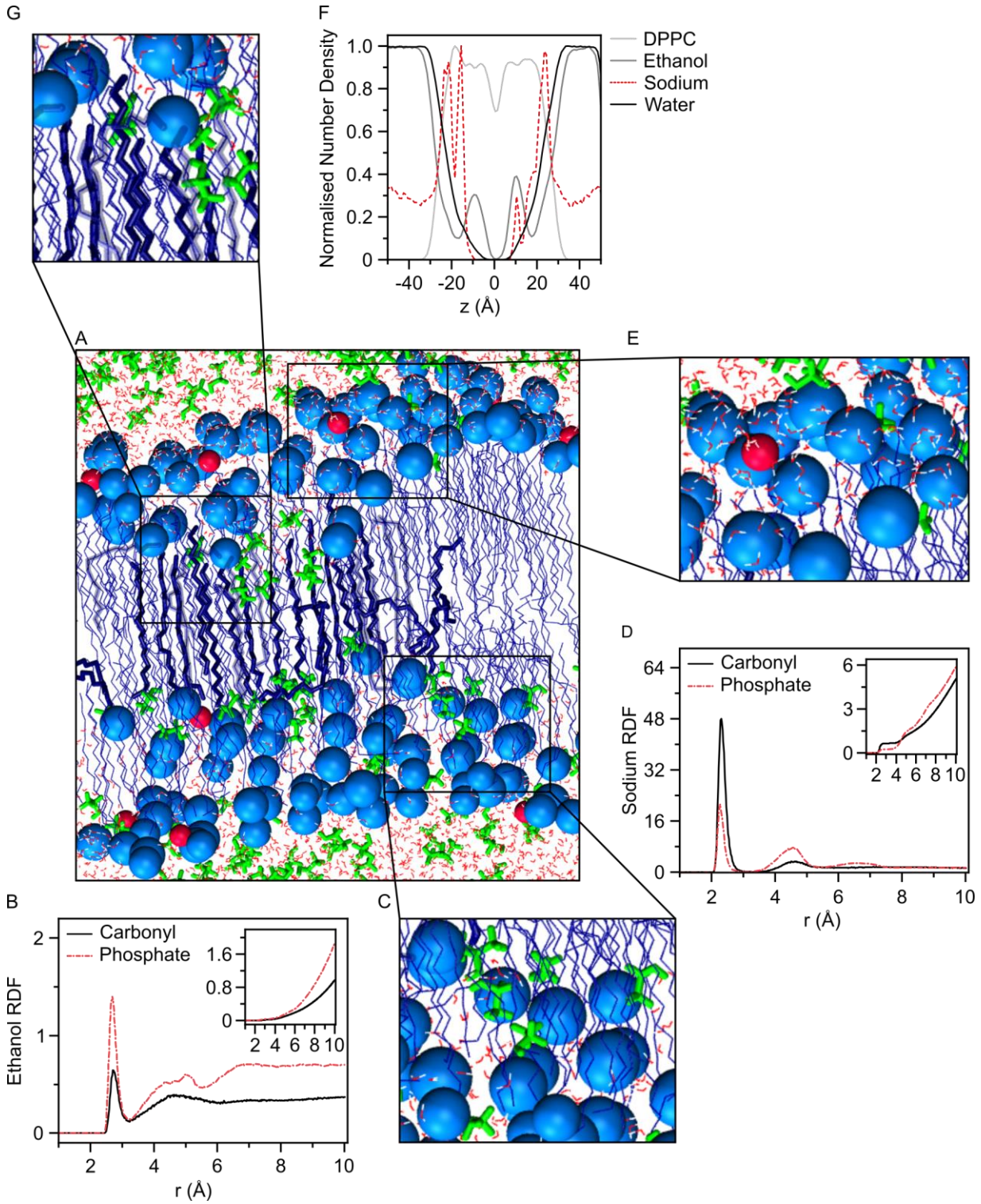

Figure 7. (A) Pictorial representation of the DPPC lipid bilayer in the presence of an aqueous solution of 0.15 M NaCl and 4 M ethanol after 600 ns MD simulations. The sodium ions and the ethanol molecules are shown in red beads and green bars, respectively, while the water molecules are depicted in red lines. The lipid headgroup is represented as light blue bead while the lipid chains are shown in blue lines. Lipid chains from the upper leaflet have been coloured in a lighter blue for clarity. (B) RDF for ethanol coordination with the carbonyl (black solid line) and phosphate (red dashed line) oxygens of DPPC and (C) zoom-in of the interactions between the lipid headgroups and ethanol

molecules. (D) RDF for Na^+ coordination with the carbonyl and phosphate oxygens of DPPC and (E) zoom-in of the interactions between the lipid headgroups and the sodium ions. In both cases, the cumulative curves of the RDFs are shown as insets. (F) Normalized number densities of DPPC (light grey), ethanol (grey), sodium ions (red, dotted) and water (black) across the bilayer. (G) Zoom-in showing lipid chains and ethanol molecules within the bilayer.

Calcium ions have higher binding affinities to lipid headgroups compared to sodium ions. In general, upon binding to lipid membranes, cations lose at least one water molecule from their hydration shell. In the presence of a lipid membrane, the most favorable state for a sodium ion is the coordination with five water molecules, while a calcium ion prefers to bind to the four lipid oxygens in the membrane.[62] The results of the 600 ns-simulations for DPPC bilayers in 0.15 and 0.6 M $CaCl_2$ are shown in **Figure 8** and **Figure S6**. We could identify a clear interdigitated region in presence of 0.15 M $CaCl_2$ (**Figure 8A**), and partial interdigitation for the 0.6 M $CaCl_2$ condition (**Figure S6A**). In this case, ethanol RDFs also showed preferential bonding to the phosphate oxygens at both 0.15 and 0.6 M $CaCl_2$ (**Figure 8B,C** and **Figure S6B,C**) in the region between 2 and 4 Å. Nevertheless, ethanol was able to penetrate deep within the bilayer, and to localize at the lipid-water interface, as shown by the peak in the number density at 40 Å (**Figure 8F,G** and **Figure S6F,G**). In analogy with the NaCl system, we found that calcium ions interacted with the lipid bilayer and calculated RDFs for Ca^{2+} coordination with the phosphate and the carbonyl oxygen of DPPC molecules (**Figure 8D,E** and **Figure S6D,E**). The cations exhibited preferential coordination to the carbonyl oxygens compared to the phosphate oxygens in the region between 2 and 4 Å at both concentrations. Furthermore, the number density profiles showed that the calcium ions remained located in proximity to the lipid-water interface (**Figure 8F,G** and **Figure S6F,G**).

Overall, binding of ethanol at the lipid-water interface and bilayer penetration occurred at all the examined conditions. From MD simulations, we observed more significant bilayer interdigitation for the 0.15 M NaCl or $CaCl_2$ systems compared to the 0.6 M NaCl or $CaCl_2$ ones. Cation binding has been shown to lead to bilayer compression and reduction in the area per lipid;[47,58] high cation concentrations may restrain ethanol-induced bilayer interdigitation, which cannot be observed in the time span of the simulations, while SAXS and WAXS measurements of DPPC bulk phases have shown bilayer interdigitation at 0.6 M NaCl and $CaCl_2$.

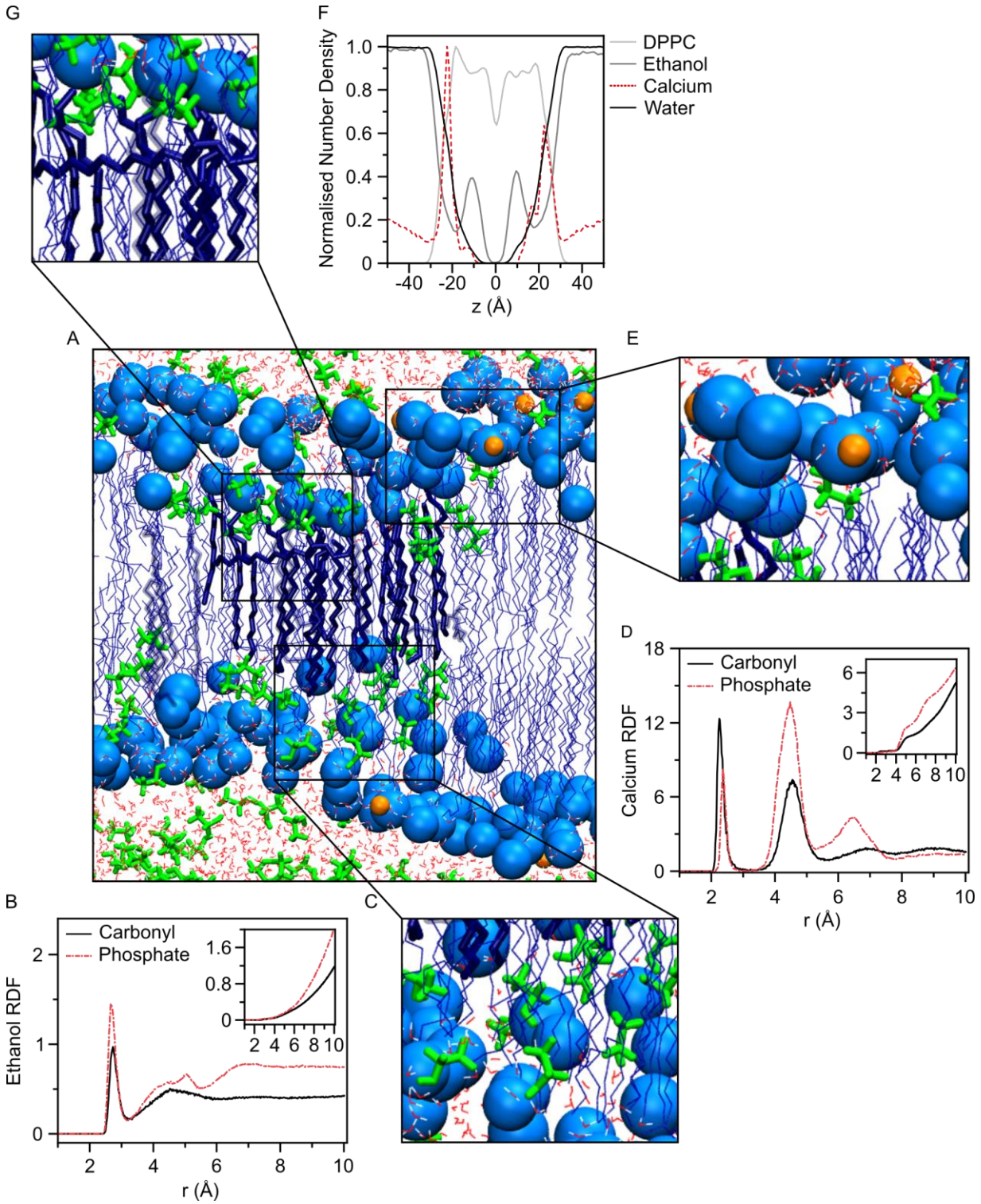

Figure 8. (A) Pictorial representation of the DPPC lipid bilayer in the presence of an aqueous solution of 0.15 M $CaCl_2$ and 4 M ethanol after 600 ns MD simulations. The calcium ions and the ethanol molecules are shown in orange beads and green bars, respectively, while the water molecules are depicted in red lines. The lipid headgroup is represented as light blue bead while the lipid chains are shown in blue. Selected lipid tails from the top (darker blue) and bottom leaflet (lighter blue) have been highlighted for clarity. (B) RDF for ethanol coordination with the carbonyl (black solid line) and phosphate (red dashed line) oxygens of DPPC and (C) zoom-in of the interactions between the

lipid headgroups and ethanol molecules. (D) RDF for Ca^{2+} coordination with the carbonyl and phosphate oxygens of DPPC and (E) zoom-in of the interactions between the lipid headgroups and the calcium ions. In both cases, the cumulative curves of the RDFs are shown as insets. (F) Normalized number densities of DPPC (light grey), ethanol (grey), calcium ions (red, dotted) and water (black) across the bilayer. (G) Zoom-in of the lipid chains in the bilayer.

CONCLUSIONS

We investigated the role of cations in ethanol-induced membrane interdigitation for bulk phase and vesicular DPPC with several techniques spanning a wide range of length scales. X-ray scattering measurements showed that bulk phase DPPC exhibited d-spacings typical of interdigitated membranes at all the NaCl and $CaCl_2$ concentrations studied when incubated with 4 M ethanol below the lipid T_m. Interestingly, broad peaks were observed at 0.15 $CaCl_2$, while lamellar ordering was restored at higher calcium concentrations. MD simulations of initial stages of the interdigitation process at selected salt concentrations showed that bilayer interdigitation was more significant for the 0.15 M NaCl or $CaCl_2$ systems compared to the 0.6 M NaCl or $CaCl_2$ ones. Additionally, MD simulations provided insights into cation and ethanol coordination to the lipid bilayer, and into the location of ethanol within the membrane. We showed preferential coordination to the carbonyl oxygen of DPPC for both sodium and calcium, whereas ethanol formed hydrogen bonding with the phosphate oxygens.

We observed a similar behaviour to the bulk phase DPPC in X-ray scattering measurements of small DPPC vesicles incubated with 4 M ethanol, and the d-spacings of vesicular DPPC were in good agreement with the bulk phase data. Neutron and X-ray scattering measurements of vesicular DPPC incubated with 4 M ethanol agreed with each other within 2-3 Å. By fitting the neutron scattering data, we obtained bilayer thicknesses of 37 Å for the majority of the salt concentrations explored. DLS measurements showed substantial vesicle aggregation upon ethanol addition for both the NaCl series and the 0.4 and 0.6 M $CaCl_2$ samples. However, DPPC vesicles containing 0.15 M $CaCl_2$ formed lamellar stacks with bilayer thicknesses of 25 Å upon ethanol addition, which was also confirmed by the sol-gel transition of the vesicle suspension and suggested vesicle fusion in interdigitated stacks.

The ethanol-induced vesicle fusion in interdigitated stacks has implications for the production of interdigitation-fusion vesicles: this method requires the formation of interdigitated lamellar sheets upon ethanol-induced vesicle fusion, which refold into large unilamellar vesicles upon increasing the temperature above the lipid T_m. Importantly, ethanol was able to induce vesicle fusion in interdigitated lamellae only in the case of 0.15 M $CaCl_2$; for the other conditions, we observed aggregation in large, multilamellar vesicles. Therefore, the choice of cation and its concentration is

crucial in this context. Here, we chose DPPC as a model lipid since it is widely used in the formulation of vesicles for drug delivery applications; future studies on mixtures of saturated PCs with different chain lengths and other divalent cations (*e.g.*, magnesium) will expand the results presented here. Overall, the work presented here furthers our understanding of the effect of ionic species on lipid membrane interdigitation, with implications for cell biology and biochemistry, and is directly applicable for *i.e.*, the fabrication of interdigitation-fusion vesicles with high entrapped volumes.

EXPERIMENTAL SECTION

Materials

1,2-dipalmitoyl-*sn*-glycero-3-phosphocholine (DPPC) was purchased from Avanti Polar Lipids (Alabaster, AL) and used as supplied. Deuterated water (D_2O) was purchased from Sigma Aldrich while the partially deuterated ethanol (CH_3CH_2OD) was kindly donated by the ISIS Deuteration Facility (Science and Technology Facilities Campus, Rutherford Appleton Laboratory, Didcot, UK). $CaCl_2$ and NaCl were purchased from VWR International.

Methods

Bulk phase samples for X-ray scattering measurements. To prepare bulk phase samples for X-ray scattering measurements, 0.8 mL of 25 mg mL^{-1} DPPC in chloroform was dried with a nitrogen gas stream in a glass vial. The lipid films were kept under vacuum overnight to remove trace solvent before hydration with 65.15 µL of aqueous solutions containing 0.15, 0.4 or 0.6 M of NaCl or $CaCl_2$. Twenty freeze-thaw cycles between -80 °C and 55 °C were performed. 19.85 µL of ethanol was then added and the resulting mixture heat cycled fifteen times between -80 °C and 55 °C. The aqueous fraction was 80.2 wt % in these mixtures. The samples were then transferred into glass capillaries by centrifugation (1500 x g for 1 min), sealed and measured within 48 h.

Vesicle samples for X-ray scattering measurements. Vesicle samples for X-ray scattering measurements were prepared as follows. DPPC lipid films were prepared by drying 0.4 mL of 25 mg mL^{-1} DPPC in chloroform with a nitrogen gas stream in a glass vial. The lipid films were kept under vacuum overnight and hydrated with 0.5 mL of aqueous solutions containing 0.15, 0.4 or 0.6 M of NaCl or $CaCl_2$ for 1 hour at 55 °C while stirring. The obtained vesicle suspensions were extruded thirty-five times through 100 and then 50 nm pore-sized membranes at 55 °C. Samples were left to cool to RT for fifteen minutes before adding pure ethanol to a final concentration of 25 vol% while stirring. Vesicle samples were transferred to polycarbonate capillaries, sealed and measured after two days.

X-ray scattering measurements. Simultaneous SAXS/WAXS measurements were carried out at 25 °C at Diamond Light Source (UK), using the I22 beamline. Samples were mounted in 1.5 mm diameter

glass (bulk phase samples) or polycarbonate (vesicle samples) capillaries (Spectrum Plastics, US). An X-ray beam with an energy of 12.5 keV and a sample to detector distance of 4.77 m were used to give a scattering vector $S = \frac{2}{\lambda} sin\left(\frac{\theta}{2}\right) = \frac{Q}{2\pi}$, where θ is the scattering angle. Images were analysed using the AXcess software package.[39] Briefly, radial integration of the two-dimensional SAXS/WAXS images gave one-dimensional diffraction patterns. A silver behenate standard was used for software calibration and Gaussian functions were used to fit the Bragg peaks, which were indexed using a lamellar model. For the vesicle samples, background subtraction was performed with the DAWN software package[63,64] in 'processing' mode using the 'subtract frame (External)' function before plotting the data; aqueous solutions of the appropriate salt concentration containing 4 M ethanol were used as blank solutions. The normalised scattering intensity was plotted as a function of the scattering vector $Q = \frac{4\pi}{\lambda} sin\left(\frac{\theta}{2}\right)$.

Dynamic light scattering measurements. Vesicle samples for DLS were diluted to 0.5 mg mL^{-1} lipid content in the appropriate aqueous salt solution. Measurements were acquired with a ZetaSizer Nano ZS (Malvern) with a scattering angle fixed at 173°. Each measurement was repeated three times, and results were averaged and normalised. Intensity distributions are reported as a function of the hydrodynamic diameter.

Vesicle samples for small-angle neutron scattering measurements. Vesicle samples for SANS were prepared as follows. Briefly, DPPC lipid films were prepared by drying 0.4 mL of 25 mg mL^{-1} DPPC in chloroform with a nitrogen gas stream in a glass vial. The lipid films were kept under vacuum overnight to remove trace solvent before hydrating with 0.5 mL of aqueous solutions containing 0.15, 0.4 or 0.6 M of NaCl or $CaCl_2$ for 1 hour at 55 °C while stirring. The hydrating solutions for SANS were prepared by dissolving the appropriate amount of salt in deuterated water (D_2O). The obtained vesicle suspensions were then extruded thirty-five times through 100 and then 50 nm pore-sized membranes at 55 °C. Samples were left to cool to RT for fifteen minutes before adding partially deuterated ethanol (CH_3CH_2OD) to a final concentration of 25 vol% while stirring. Vesicle samples were transferred into 1 mm path length quartz cuvette cells prior to measurement.

Small-Angle Neutron Scattering. Measurements were performed at the SANS2D beamline of the ISIS pulsed neutron source at the Rutherford Appleton Laboratory (Didcot, UK) using a sample changer and water bath at 25 °C. The pinhole collimation was set to $L_1 = L_2 = 4$ m while sample-detector distances were configured to give a scattering vector $Q = \frac{4\pi}{\lambda} sin\left(\frac{\theta}{2}\right)$ range of 0.004 to 0.722 $Å^{-1}$, where θ is the scattering angle and neutrons of wavelengths λ of 1.75 to 16.5 Å were used by the time of flight technique. Data reduction was performed using MantidPlot[65] and the SANS curves were fitted with SasView v4.1.0.[66] The solvent scattering length density $SLD_{solv,final}$ was calculated by:

$$SLD_{solv,final} = SLD_{CH3CH2OD} * x_{vol,CH3CH2OD} + SLD_{D2O} * x_{vol,D2o} \quad (1),$$

Where $SLD_{CH3CH2OD}$ is the scattering length density of partially deuterated ethanol, $x_{vol,CH3CH2OD}$ is its volume fraction, and SLD_{D2O} and $x_{vol,D2o}$ are the scattering length density and the volume fraction of deuterated water, respectively. The scattering length density (SLD) calculator plug-in of SasView was used to calculate $SLD_{CH3CH2OD}$. The obtained values were $SLD_{CH3CH2OD}$ = 7.29E^{-07} Å^{-2} and $SLD_{solv,final}$ = 4.96E^{-06} Å^{-2}.

Molecular dynamics simulations. To understand the structure and dynamics of the DPPC lipid bilayer in the presence of ethanol and ions, four different bilayer models with 72 DPPC lipid molecules in each leaflet in aqueous solutions containing 0.15 or 0.6 M NaCl or $CaCl_2$ were simulated. Two ethanol molecules per lipid molecule were used as part of the buffer, based on previous work.[67] Fifty water molecules per lipid were added to each system. The final size of the simulation system was 6.6 × 6.6 × 10.4 nm^3 with approximately 40,000 atoms. The models were created with the CHARMM Gui and VMD software packages.[68,69] MD simulations for the DPPC model systems were run using NAMD code[70] with CHARMM36 forcefield parameters and the TIP3P water model[71] to solvate the lipid molecules. A particle – mesh Ewald algorithm was used to compute the long range electrostatic interactions with periodic boundary conditions.[72] A force-switching function was used to switch off the Lennard-Jones potential within 10-12 Å, together with a non-bonded pair list cut-off of 16 Å and a 2 fs timestep. After the initial energy minimization, the DPPC lipid molecules were released with 5, 2, 1, 0.5 and 0.1 kcal mol^{-1} position restraint on phosphate atoms, with systems at each restraint step equilibrated for 1 ns in the NPT ensemble. Following this, an MD simulation for each system was run for 600 ns without any constraints. The temperature and pressure were maintained at 298 K and 1 atm, respectively, *via* Langevin coupling with a damping coefficient of 5 ps^{-1}. The data analyses were performed for the last 300 ns of the simulations unless specified otherwise.

CONFLICTS OF INTEREST

There are no conflicts of interest to declare.

ACKNOWLEDGEMENTS

I.Y. and M.M.S. acknowledge the Australian Research Council for financial support under the Discovery Project scheme [DP140101888 and DP170100511]. This research was undertaken with the assistance of resources from the National Computational Infrastructure (NCI) [e87], Australia. V.N. acknowledges the Ermenegildo Zegna Founder's Scholarship. V.N. and M.M.S. acknowledge support from the Rosetrees Trust. M.N.H. acknowledges the support from the FP7 Marie Curie Intra-European Fellowship "SMase LIPOSOME" (626766). This research is published with the support of the Swiss National Science Foundation (P300PA_171540). H.M.G.B. acknowledges support from

the H2020 through the Individual Marie Skłodowska-Curie Fellowship "SmartCubes (703666). Experiments at the ISIS Neutron and Muon Source were supported by a beamtime allocation from the Science and Technology Facilities Council (RB1810203 and RB1810329). This work benefited from the use of the SasView application, originally developed under NSF award DMR-0520547. SasView contains code developed with funding from the European Union's Horizon 2020 research and innovation programme under the SINE2020 project, grant agreement 654000. We acknowledge Diamond Light Source for provision of synchrotron beamtime (SM 18658) and we would like to thank Dr. Andy Smith for assistance using beamline I22. Experimental raw data are available upon request from rdm-enquiries@imperial.ac.uk. Molecular simulation data is available upon reasonable request from irene.yarovsky@rmit.edu.au.

REFERENCES

1. Et-Thakafy, O. *et al.* Mechanical Properties of Membranes Composed of Gel-Phase or Fluid-Phase Phospholipids Probed on Liposomes by Atomic Force Spectroscopy. *Langmuir* **33**, 5117–5126 (2017).
2. Hatta, I., Kato, S. & Takahashi, H. Phase transitions and polymorphism in phospholipids. *Phase Transitions* **45**, 157–184 (1993).
3. Slater, J. L. & Huang, C.-H. Interdigitated bilayer membranes. *Prog. Lipid Res.* **27**, 325–359 (1988).
4. Goto, M. *et al.* Chain elongation of diacylphosphatidylcholine induces fully bilayer interdigitation under atmospheric pressure. *Colloids Surfaces B Biointerfaces* **84**, 44–48 (2011).
5. Matsuki, H., Goto, M., Tada, K. & Tamai, N. Thermotropic and Barotropic Phase Behavior of Phosphatidylcholine Bilayers. *International Journal of Molecular Sciences* **14**, (2013).
6. Neuhaus, F. *et al.* Vesicle Origami: Cuboid Phospholipid Vesicles Formed by Template-Free Self-Assembly. *Angew. Chemie Int. Ed.* **56**, 6515–6518 (2017).
7. Oliveira, T. R. *et al.* Temperature-Dependence of Cationic Lipid Bilayer Intermixing: Possible Role of Interdigitation. *Langmuir* **28**, 4640–4647 (2012).
8. Ryhänen, S. J., Alakoskela, J.-M. I. & Kinnunen, P. K. J. Increasing Surface Charge Density Induces Interdigitation in Vesicles of Cationic Amphiphile and Phosphatidylcholine. *Langmuir* **21**, 5707–5715 (2005).
9. Smith, E. A., van Gorkum, C. M. & Dea, P. K. Properties of phosphatidylcholine in the presence of its monofluorinated analogue. *Biophys. Chem.* **147**, 20–27 (2010).
10. Goto, M. *et al.* Comprehensive characterization of temperature- and pressure-induced bilayer phase transitions for saturated phosphatidylcholines containing longer chain homologs. *Colloids Surfaces B Biointerfaces* **128**, 389–397 (2015).
11. Hata, T., Matsuki, H. & Kaneshina, S. Effect of local anesthetics on the phase transition temperatures of ether- and ester-linked phospholipid bilayer membranes. *Colloids Surfaces B Biointerfaces* **18**, 41–50 (2000).
12. Wu, F.-G., Wang, N.-N., Tao, L.-F. & Yu, Z.-W. Acetonitrile Induces Nonsynchronous Interdigitation and Dehydration of Dipalmitoylphosphatidylcholine Bilayers. *J. Phys. Chem. B* **114**, 12685–12691 (2010).

13. Löbbecke, L. & Cevc, G. Effects of short-chain alcohols on the phase behavior and interdigitation of phosphatidylcholine bilayer membranes. *Biochim. Biophys. Acta - Biomembr.* **1237**, 59–69 (1995).

14. Di Rocco, G., Baldari, S., Pani, G. & Toietta, G. Stem cells under the influence of alcohol: effects of ethanol consumption on stem/progenitor cells. *Cell. Mol. Life Sci.* **76**, 231–244 (2019).

15. Vanegas, J. M., Contreras, M. F., Faller, R. & Longo, M. L. Role of Unsaturated Lipid and Ergosterol in Ethanol Tolerance of Model Yeast Biomembranes. *Biophys. J.* **102**, 507–516 (2012).

16. Nainwal, N., Jawla, S., Singh, R. & Saharan, V. A. Transdermal applications of ethosomes – a detailed review. *J. Liposome Res.* **29**, 103–113 (2019).

17. Lim, S. W. Z., Wong, Y. S., Czarny, B. & Venkatraman, S. Microfluidic-directed self-assembly of liposomes: Role of interdigitation. *J. Colloid Interface Sci.* **578**, 47–57 (2020).

18. Ahl, P. L. *et al.* Interdigitation-fusion: a new method for producing lipid vesicles of high internal volume. *Biochim. Biophys. Acta - Biomembr.* **1195**, 237–244 (1994).

19. Paleos, C. M., Tsiourvas, D., Sideratou, Z. & Pantos, A. Formation of artificial multicompartment vesosome and dendrosome as prospected drug and gene delivery carriers. *J. Control. Release* **170**, 141–152 (2013).

20. Kisak, E. T., Coldren, B. & Zasadzinski, J. A. Nanocompartments Enclosing Vesicles, Colloids, and Macromolecules via Interdigitated Lipid Bilayers. *Langmuir* **18**, 284–288 (2002).

21. Forbes, N., Shin, J. E., Ogunyankin, M. & Zasadzinski, J. A. Inside-outside self-assembly of light-activated fast-release liposomes. *Phys. Chem. Chem. Phys.* **17**, 15569–15578 (2015).

22. Barry, J. A. & Gawrisch, K. Direct NMR Evidence for Ethanol Binding to the Lipid-Water Interface of Phospholipid Bilayers. *Biochemistry* **33**, 8082–8088 (1994).

23. Patra, M. *et al.* Under the Influence of Alcohol: The Effect of Ethanol and Methanol on Lipid Bilayers. *Biophys. J.* **90**, 1121–1135 (2006).

24. Ingólfsson, H. I. & Andersen, O. S. Alcohol's Effects on Lipid Bilayer Properties. *Biophys. J.* **101**, 847–855 (2011).

25. Vierl, U., Löbbecke, L., Nagel, N. & Cevc, G. Solute effects on the colloidal and phase behavior of lipid bilayer membranes: ethanol-dipalmitoylphosphatidylcholine mixtures. *Biophys. J.* **67**, 1067–1079 (1994).

26. LENEVEU, D. M., RAND, R. P. & PARSEGIAN, V. A. Measurement of forces between lecithin bilayers. *Nature* **259**, 601 (1976).

27. LeNeveu, D. M. & Rand, R. P. Measurement and modification of forces between lecithin bilayers. *Biophys. J.* **18**, 209–230 (1977).

28. Marra, J. & Israelachvili, J. Direct measurements of forces between phosphatidylcholine and phosphatidylethanolamine bilayers in aqueous electrolyte solutions. *Biochemistry* **24**, 4608–4618 (1985).

29. Petrache, H. I., Zemb, T., Belloni, L. & Parsegian, V. A. Salt screening and specific ion adsorption determine neutral-lipid membrane interactions. *Proc. Natl. Acad. Sci.* **103**, 7982 LP – 7987 (2006).

30. Alsop, R. J., Maria Schober, R. & Rheinstädter, M. C. Swelling of phospholipid membranes by divalent metal ions depends on the location of the ions in the bilayers. *Soft Matter* **12**, 6737–6748 (2016).

31. Shahane, G., Ding, W., Palaiokostas, M. & Orsi, M. Physical properties of model biological lipid bilayers: insights from all-atom molecular dynamics simulations. *J. Mol. Model.* **25**, 76 (2019).

32. Lin, X., Nair, V., Zhou, Y. & Gorfe, A. A. Membrane potential and dynamics in a ternary lipid mixture: insights from molecular dynamics simulations. *Phys. Chem. Chem. Phys.* **20**, 15841–15851 (2018).

33. Sachs, J. N. & Woolf, T. B. Understanding the Hofmeister Effect in Interactions between Chaotropic Anions and Lipid Bilayers: Molecular Dynamics Simulations. *J. Am. Chem. Soc.* **125**, 8742–8743 (2003).

34. Hong, C., Tieleman, D. P. & Wang, Y. Microsecond Molecular Dynamics Simulations of Lipid Mixing. *Langmuir* **30**, 11993–12001 (2014).

35. Khatami, M. H., Saika-Voivod, I. & Booth, V. All-atom molecular dynamics simulations of lung surfactant protein B: Structural features of SP-B promote lipid reorganization. *Biochim. Biophys. Acta - Biomembr.* **1858**, 3082–3092 (2016).

36. Baker, M. K. & Abrams, C. F. Dynamics of Lipids, Cholesterol, and Transmembrane α-Helices from Microsecond Molecular Dynamics Simulations. *J. Phys. Chem. B* **118**, 13590–13600 (2014).

37. Holme, M. N. *et al.* Fate of Liposomes in the Presence of Phospholipase C and D: From Atomic to Supramolecular Lipid Arrangement. *ACS Cent. Sci.* **4**, 1023–1030 (2018).

38. Thewalt, J. L. & Bloom, M. Phosphatidylcholine: cholesterol phase diagrams. *Biophys. J.* **63**, 1176–1181 (1992).

39. M, S. J. *et al.* Pressure-jump X-ray studies of liquid crystal transitions in lipids. *Philos. Trans. R. Soc. A Math. Phys. Eng. Sci.* **364**, 2635–2655 (2006).

40. Simon, S. A. & McIntosh, T. J. Interdigitated hydrocarbon chain packing causes the biphasic transition behavior in lipid/alcohol suspensions. *Biochim. Biophys. Acta - Biomembr.* **773**, 169–172 (1984).

41. Sun, W. J., Tristram-Nagle, S., Suter, R. M. & Nagle, J. F. Structure of gel phase saturated lecithin bilayers: temperature and chain length dependence. *Biophys. J.* **71**, 885–891 (1996).

42. Larsson, K. & Quinn, P. Physical Properties — Structural and Physical Characteristics. in 465–484 (1994). doi:10.1007/978-1-4899-2905-1_8

43. Komatsu, H. & Okada, S. Ethanol-induced aggregation and fusion of small phosphatidylcholine liposome: participation of interdigitated membrane formation in their processes. *Biochim. Biophys. Acta - Biomembr.* **1235**, 270–280 (1995).

44. Nele, V. *et al.* Effect of Formulation Method, Lipid Composition, and PEGylation on Vesicle Lamellarity: A Small-Angle Neutron Scattering Study. *Langmuir* **35**, 6064–6074 (2019).

45. Rappolt, M. *Chapter 9 The Biologically Relevant Lipid Mesophases as "Seen" by X-Rays. Advances in Planar Lipid Bilayers and Liposomes* **5**, (2006).

46. Adachi, T., Takahashi, H., Ohki, K. & Hatta, I. Interdigitated structure of phospholipid-alcohol systems studied by x-ray diffraction. *Biophys. J.* **68**, 1850–1855 (1995).

47. Pabst, G. *et al.* Rigidification of Neutral Lipid Bilayers in the Presence of Salts. *Biophys. J.* **93**, 2688–2696 (2007).

48. Mou, J., Yang, J., Huang, C. & Shao, Z. Alcohol Induces Interdigitated Domains in Unilamellar Phosphatidylcholine Bilayers. *Biochemistry* **33**, 9981–9985 (1994).

49. Ly, H. V, Block, D. E. & Longo, M. L. Interfacial Tension Effect of Ethanol on Lipid Bilayer

Rigidity, Stability, and Area/Molecule: A Micropipet Aspiration Approach. *Langmuir* **18**, 8988–8995 (2002).

50. Schmiedel, H., Almásy, L. & Klose, G. Multilamellarity, structure and hydration of extruded POPC vesicles by SANS. *Eur. Biophys. J.* **35**, 181–189 (2006).

51. TATULIAN, S. A. Binding of alkaline-earth metal cations and some anions to hosphatidylcholine liposomes. *Eur. J. Biochem.* **170**, 413–420 (1987).

52. Chapman, D., Peel, W. E., Kingston, B. & Lilley, T. H. Lipid phase transitions in model biomembranes: The effect of ions on phosphatidylcholine bilayers. *Biochim. Biophys. Acta - Biomembr.* **464**, 260–275 (1977).

53. Binder, H. & Zschörnig, O. The effect of metal cations on the phase behavior and hydration characteristics of phospholipid membranes. *Chem. Phys. Lipids* **115**, 39–61 (2002).

54. McManus, J. J., Rädler, J. O. & Dawson, K. A. Does Calcium Turn a Zwitterionic Lipid Cationic? *J. Phys. Chem. B* **107**, 9869–9875 (2003).

55. Lis, L. J., Parsegian, V. A. & Rand, R. P. Binding of divalent cations to dipalmitoylphosphatidylcholine bilayers and its effect on bilayer interaction. *Biochemistry* **20**, 1761–1770 (1981).

56. Boni, L. T. *et al.* Curvature dependent induction of the interdigitated gel phase in DPPC vesicles. *Biochim. Biophys. Acta - Biomembr.* **1146**, 247–257 (1993).

57. McConnell, D. S. & Schullery, S. E. Phospholipid vesicle fusion and drug loading: temperature, solute and cholesterol effects, and, a rapid preparation for solute-loaded vesicles. *Biochim. Biophys. Acta - Biomembr.* **818**, 13–22 (1985).

58. Gurtovenko, A. A. & Vattulainen, I. Effect of NaCl and KCl on Phosphatidylcholine and Phosphatidylethanolamine Lipid Membranes: Insight from Atomic-Scale Simulations for Understanding Salt-Induced Effects in the Plasma Membrane. *J. Phys. Chem. B* **112**, 1953–1962 (2008).

59. Dickey, A. N. & Faller, R. How Alcohol Chain-Length and Concentration Modulate Hydrogen Bond Formation in a Lipid Bilayer. *Biophys. J.* **92**, 2366–2376 (2007).

60. Gurtovenko, A. A. & Anwar, J. Interaction of Ethanol with Biological Membranes: The Formation of Non-bilayer Structures within the Membrane Interior and their Significance. *J. Phys. Chem. B* **113**, 1983–1992 (2009).

61. Jurkiewicz, P., Cwiklik, L., Vojtíšková, A., Jungwirth, P. & Hof, M. Structure, dynamics, and hydration of POPC/POPS bilayers suspended in NaCl, KCl, and CsCl solutions. *Biochim. Biophys. Acta - Biomembr.* **1818**, 609–616 (2012).

62. Yang, J., Calero, C., Bonomi, M. & Martí, J. Specific Ion Binding at Phospholipid Membrane Surfaces. *J. Chem. Theory Comput.* **11**, 4495–4499 (2015).

63. Filik, J. *et al.* Processing two-dimensional X-ray diffraction and small-angle scattering data in {\it DAWN 2}. *J. Appl. Crystallogr.* **50**, 959–966 (2017).

64. Basham, M. *et al.* Data Analysis WorkbeNch (DAWN). *J. Synchrotron Radiat.* **22**, 853–858 (2015).

65. Arnold, O. *et al.* Mantid—Data analysis and visualization package for neutron scattering and μ SR experiments. *Nucl. Instruments Methods Phys. Res. Sect. A Accel. Spectrometers, Detect. Assoc. Equip.* **764**, 156–166 (2014).

66. SASView reference. Available at: http://www.sasview.org/.

67. Kranenburg, M. & Smit, B. Simulating the effect of alcohol on the structure of a membrane.

FEBS Lett. **568**, 15–18 (2004).

68. Jo, S., Kim, T., Iyer, V. G. & Im, W. CHARMM-GUI: A web-based graphical user interface for CHARMM. *J. Comput. Chem.* **29**, 1859–1865 (2008).

69. Humphrey, W., Dalke, A. & Schulten, K. VMD: Visual molecular dynamics. *J. Mol. Graph.* **14**, 33–38 (1996).

70. Phillips, J. C. *et al.* Scalable molecular dynamics with NAMD. *J. Comput. Chem.* **26**, 1781–1802 (2005).

71. Jorgensen, W. L., Chandrasekhar, J., Madura, J. D., Impey, R. W. & Klein, M. L. Comparison of simple potential functions for simulating liquid water. *J. Chem. Phys.* **79**, 926–935 (1983).

72. Darden, T., York, D. & Pedersen, L. Particle mesh Ewald: An N·log(N) method for Ewald sums in large systems. *J. Chem. Phys.* **98**, 10089–10092 (1993).

Peer reviewed version of the manuscript published in final form at Langmuir (2021)

Supporting Information

Design of lipid-based nanocarriers via cation modulation of ethanol-interdigitated lipid membranes

Valeria Nele[1], Margaret N. Holme[1,2], M. Harunur Rashid[3,4], Hanna M. G. Barriga[2], Tu C. Le[3], Michael R. Thomas[1,6], James J. Doutch[5], Irene Yarovsky[3]*, Molly M. Stevens[1,2]**

[1]Department of Materials, Department of Bioengineering and Institute of Biomedical Engineering Imperial College London, London, SW7 2AZ, UK

[2]Department of Medical Biochemistry and Biophysics, Karolinska Institutet, SE-171 77 Stockholm, Sweden

[3]School of Engineering, RMIT University, Melbourne, Victoria, 3001, Australia

[4]Department of Mathematics and Physics, North South University, Bashundhara, Dhaka, 1229, Bangladesh

[5]ISIS Neutron and Muon Source, STFC, Rutherford Appleton Laboratory, Didcot, OX11 ODE, UK

[6]London Centre for Nanotechnology and Department of Biochemical Engineering, University College London, 17−19 Gordon Street, London, WC1H 0AH, UK

Correspondence to:

* Email: irene.yarovsky@rmit.edu.au ** Email: m.stevens@imperial.ac.uk

Neutron scattering data were fitted using several models in the SasView v4.1.0 program. It provides the form factor P(**Q**), defined as:

$$P(\boldsymbol{Q}) = \frac{1}{V}F(\boldsymbol{Q})F'(\boldsymbol{Q}) \quad (S1)$$

With $F(\boldsymbol{Q}) = \iiint dV\rho(\boldsymbol{r})e^{-iQr}$, where $\rho(\boldsymbol{r})$ is the scattering length density at a given point in space, V is the scatterer volume and $\boldsymbol{Q}$ is the scattering vector, defined as the difference between the two wavevectors of incoming and scattered neutrons. A more detailed description of each model is reported below.

Broad Peak model. The 1D scattering intensity is calculated as:

$$I(\boldsymbol{Q}) = \frac{A}{\boldsymbol{Q}^n} + \frac{C}{1 + (|\boldsymbol{Q} - \boldsymbol{Q}_0|\xi)^m} + bkg \quad (S2)$$

where ξ is the Lorentzian screening length, m is the Lorentzian exponent (fixed as 2 in the fittings), A and C are scaling factors for the Porod and the Lorentz terms, respectively, n is the Porod exponent and $\boldsymbol{Q}_0$ is the peak position. The peak position can be used to calculate the d-spacing ($d = 2\pi/\boldsymbol{Q}_0$), which is the sum of the bilayer thickness and the coordinated water layer.

Multilayer Vesicle model. The 1D scattering intensity $I(Q)$ is calculated as the sum of a form factor $P(Q)$ normalised by the particle volume and a flat background to account for incoherent scattering:

$$I(Q) = \kappa * P(Q) + background \quad (S3),$$

where κ is a scale factor. The form factor $P(Q)$ is defined as:

$$P(Q) = \frac{\varphi}{V(R_N)}F^2(Q) \quad (S4)$$

and

$$F(Q) = (\rho_{shell} - \rho_{solv})\sum_{i=1}^{N}\left[3V(r_i)\frac{\sin(qr_i) - qr_i\cos(qr_i)}{(qr_i)^3} - 3V(R_i)\frac{\sin(qR_i) - qR_i\cos(qR_i)}{(qR_i)^3}\right] (S5).$$

Here, $r_i = r_c + (i-1)(t_s + t_w)$ is the sphere radius before shell i and is the sum of the core radius r_c and the appropriate shell and water layer thicknesses t_s and t_w, $R_i = r_i + t_s$ is the radius of a sphere with i shells, φ is the volume fraction of the ensembles, $V(r)$ is the volume of a sphere of radius r, ρ_{shell} and ρ_{solv} are the SLDs of the shell and the solvent, respectively.

Supplementary Tables

Table S1. D-spacings of bulk phase DPPC in NaCl. Fitted d-spacings of DPPC bulk mixtures equilibrated with 4 M ethanol and aqueous solutions containing 0.15, 0.4, and 0.6 M NaCl.

[NaCl] / M	d-spacing / Å
0.15	48.98 ± 0.01
0.40	48.95 ± 0.01
0.60	48.90 ± 0.01

Table S2. D-spacings of DPPC vesicles in NaCl. Fitted d-spacings of DPPC vesicles containing aqueous solutions of 0.15, 0.4, and 0.6 M NaCl and subsequently incubated with 4 M ethanol.

[NaCl] / M	d-spacing / Å
0.15	49.02 ± 0.16
0.40	49.22 ± 0.36
0.60	49.55 ± 0.38

Neutron scattering data of DPPC vesicles hydrated with 0.15, 0.4, and 0.6 M NaCl and incubated with 4 M of CH_3CH_2OD were first fitted with a Broad Peak model (see **Equation S2**). This model

combines a Lorentzian-peak function and a power law decay. The Lorentzian-peak function is one of the most common peak shape functions and is used to determine the position, the shape and the width of a peak.[1] The characteristic distance between the scattering entities (*i.e.* d-spacing) can be calculated from the peak position as: $d = \frac{2\pi}{Q}$. The power law function is a generalisation of the Porod's law and describes the scattering of fractal objects. Estimates of the Porod exponent *n* provide insights into the nature of the scattering ensembles. The scattering objects can be regarded as mass fractals ($n < 3$) or as surface fractals ($4 < n < 3$). Furthermore, for $n = 2$ the system comprises Gaussian polymer chains or two-dimensional structures such as lamellae, while for $n = 1$ the scattering objects are long rods. Porod exponents of 3 and 4 are representative of rough surfaces or particles with smooth surfaces, respectively.[2]

Table S3. Fitting parameters for DPPC vesicles in NaCl obtained from the BroadPeak model. Fitting parameters for DPPC vesicles containing 0.15, 0.4 and 0.6 M NaCl and equilibrated with 4 M CH_3CH_2OD. Here, *n* is the Porod exponent, Q_0 indicates the Bragg peak position, *A* and *C* are the scaling factors of the Porod and Lorentz terms, and ξ is the Lorentz screening length, which is related to the width of the peak. The Lorentz exponent was fixed to 2.

[NaCl] / M	*n*	Q_0 / Å^{-1}	d-spacing / Å	ξ / Å	*A* (x E^{-05})	*C*
0.15	3.23 ± 0.009	0.12 ± 0.001	52.36	47.22 ± 4.87	3.59 ± 0.12	0.22 ± 0.007
0.4	3.23 ± 0.013	0.12 ± 0.001	52.36	47.19 ± 5.81	3.58 ± 0.18	0.23 ± 0.008
0.6	3.00 ± 0.009	0.12 ± 0.001	52.36	53.87 ± 3.03	1.39 ± 0.05	0.04 ± 0.001

The neutron scattering data of DPPC vesicles hydrated with 0.15, 0.4 and 0.6 M NaCl and incubated with 4 M of CH_3CH_2OD were also fitted with a Multilayer Vesicle model (see **Equations S3-5**). A

Gaussian distribution of 10% for the number of shells and the bilayer thickness was used in this case. The fitted number of shells was rounded up to the closest integer as a non-integer value is physically impossible.

Table S4. Fitting parameters for DPPC vesicles in NaCl obtained from the Multilayer Vesicle model. Fitting parameters obtained from a Multilayer Vesicle model for DPPC vesicles containing 0.15 M, 0.4 M or 0.6 M NaCl and equilibrated with 4 M CH_3CH_2OD. Here, r_c represents the core radius, n is the number of shells surrounding the aqueous core, and t_s and t_w are the bilayer and the water layer thickness, respectively.

	Multilayer Vesicle Model			
[NaCl] / M	r_c / Å	t_s / Å	t_w / Å	n
0.15	948 ± 0.70	37 ± 0.30	13 ± 0.35	5 ± 0.03
0.4	946 ± 1.10	37 ± 0.49	12 ± 0.49	5 ± 0.05
0.6	948 ± 0.89	37 ± 0.46	13 ± 0.48	5 ± 0.04

Table S5. DLS measurements of DPPC vesicles in NaCl before and after ethanol addition. The Z-average diameter and the PDI are reported.

	Before ethanol addition		After ethanol addition	
[NaCl] / M	Z-average diameter / nm	PDI	Z-average diameter / nm	PDI
0.15	62.64 ± 12.64	0.041	1257	0.798
0.4	62.29 ± 13.14	0.044	1098	1.000
0.6	63.86 ± 16.52	0.067	1097	1.000

Table S6. D-spacings of bulk phase DPPC in $CaCl_2$. Fitted d-spacings of DPPC bulk mixtures equilibrated with 4 M ethanol and aqueous solutions containing 0.4 and 0.6 M $CaCl_2$.

[$CaCl_2$] / M	d-spacing / Å
0.40	50.54 ± 0.02
0.60	48.36 ± 0.00

Table S7. D-spacings of DPPC vesicles in $CaCl_2$. Fitted d-spacings of DPPC vesicles containing aqueous solutions containing 0.4 and 0.6 M $CaCl_2$ and subsequently incubated with 4 M ethanol at 25 °C.

[$CaCl_2$] / M	d-spacing / Å
0.4	49.64 ± 0.28
0.6	48.69 ± 0.10

Neutron scattering data of DPPC vesicles hydrated with 0.15, 0.4 and 0.6 M $CaCl_2$ and incubated with 4 M of CH_3CH_2OD were also fitted with a Broad Peak model (see **Equation S2**).

Table S8. Fitting parameters for DPPC vesicles in $CaCl_2$ obtained from the BroadPeak model. Fitting parameters for DPPC vesicles containing 0.4 and 0.6 M $CaCl_2$ and equilibrated with 4 M CH_3CH_2OD at 25 °C. Here, n is the Porod exponent, Q_0 indicates the Bragg peak position, A and C are the scaling factors of the Porod and Lorentz terms, and ξ is the Lorentz screening length, which is related to the width of the peak. The Lorentz exponent was fixed to 2.

[$CaCl_2$] / M	n	Q_0 / Å^{-1}	d-spacing / Å	ξ / Å	A (x E^{-05})	C
0.4	2.97 ± 0.014	0.12 ± 0.001	52.36	41.32 ± 4.63	1.57 ± 0.09	0.04 ± 0.002
0.6	3.80 ± 0.014	0.13 ± 0.002	48.33	556.21 ± 80.9	0.31 ± 0.002	3.15 ± 0.49

We then used the Multilayer Vesicle model (see **Equations S3-5**) to fit the neutron scattering data of DPPC vesicles hydrated with 0.6 M $CaCl_2$ and incubated with 4 M of CH_3CH_2OD. A Gaussian distribution of 10% for the number of shells and the bilayer thickness was used in this case. The fitted number of shells was rounded up to the closest integer as a non-integer value is physically impossible.

Table S9. Fitting parameters for DPPC vesicles in 0.6 M $CaCl_2$ obtained from the Multilayer Vesicle model. Fitting parameters obtained from a Multilayer Vesicle model for DPPC vesicles containing 0.6 M $CaCl_2$ and equilibrated with 4 M CH_3CH_2OD at 25°C. Here, r_c represents the core radius, n is the number of shells surrounding the aqueous core, and t_s and t_w are the bilayer and the water layer thickness, respectively.

	Multilayer Vesicle Model			
[$CaCl_2$] / M	r_c / Å	t_s / Å	t_w / Å	n
0.6	2109 ± 4.38	37 ± 0.35	12 ± 0.46	15 ± 0.38

Table S10. DLS measurements of DPPC vesicles in $CaCl_2$ before and after ethanol addition. The Z-average diameter and the PDI are reported.

	Before ethanol addition		After ethanol addition	
[$CaCl_2$] / M	Z-average diameter / nm	PDI	Z-average diameter / nm	PDI
0.4	139	0.817	2079	1.000
0.6	810	0.617	1369	0.939

Supplementary Figures

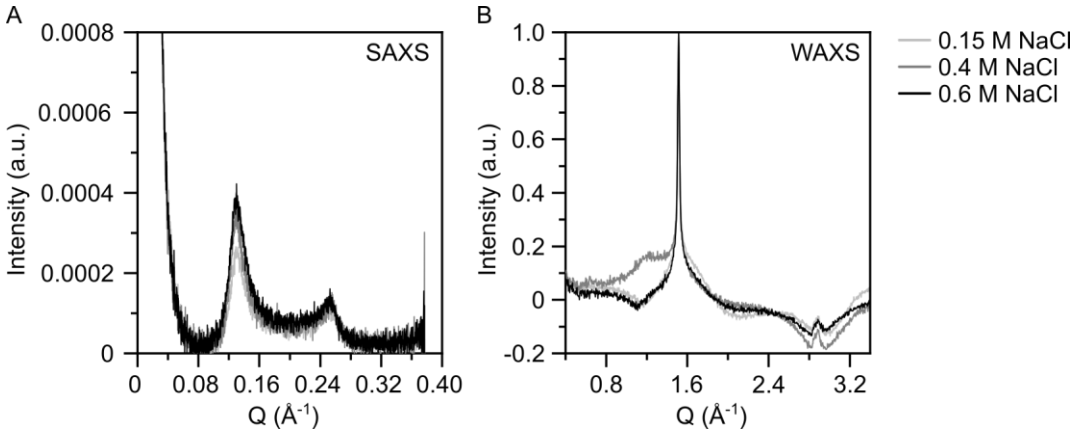

Figure S1. SAXS (A) and WAXS (B) measurements of DPPC vesicles containing aqueous solutions of 0.15, 0.4 and 0.6 M NaCl and subsequently incubated with 4 M ethanol at 25 °C. Measurements were carried out at 25 °C in polycarbonate capillaries. The reduced scattering intensity of vesicle samples compared to the bulk mixtures may be ascribed to a lower sample concentration and fewer repeat units.

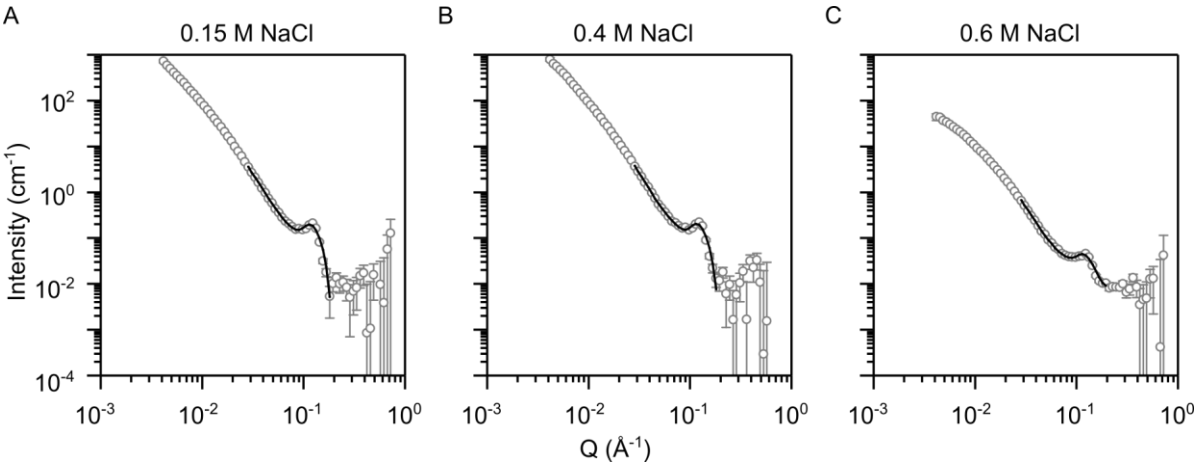

Figure S2. Neutron scattering data of DPPC vesicles containing 0.15 M (A), 0.4 M (B) and 0.6 M (C) NaCl and equilibrated with 4 M CH_3CH_2OD at 25 °C. Prior to CH_3CH_2OD addition, the vesicles were extruded 35 times through 100 nm and 50 nm pore-sized membranes. Points with errors represent measured data while lines represent fits obtained with a Multilayer Vesicle model. Data are plotted on a log-log scale.

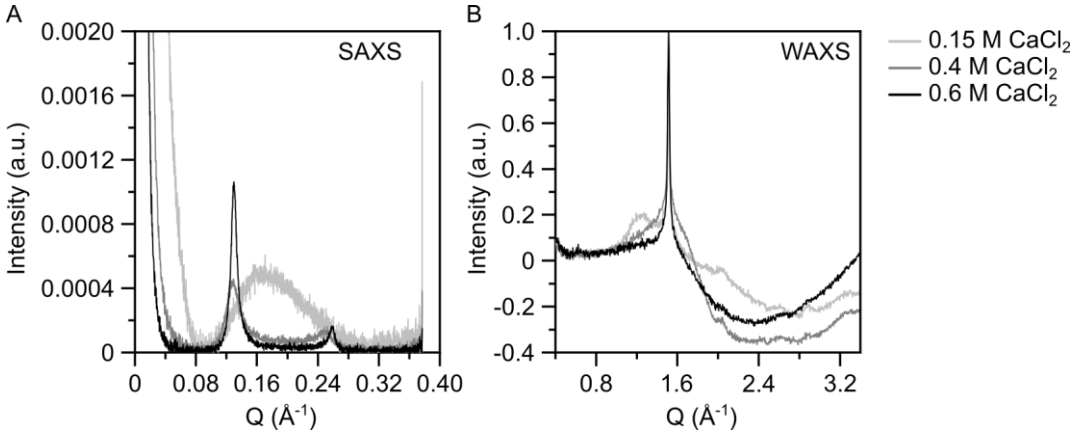

Figure S3. SAXS (A) and WAXS (B) measurements of DPPC vesicles containing aqueous solutions containing 0.15, 0.4 and 0.6 M $CaCl_2$ and subsequently incubated with 4 M ethanol. Measurements were carried out at 25 °C.

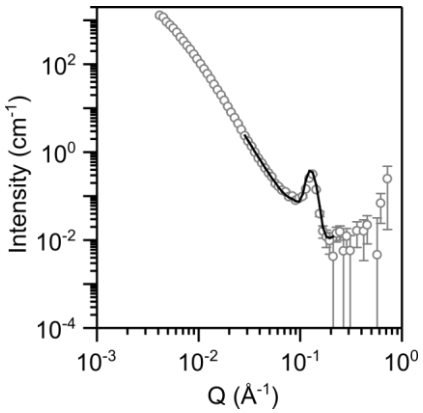

Figure S4. Neutron scattering data of DPPC vesicles containing 0.6 M $CaCl_2$ and equilibrated with 4 M CH_3CH_2OD at 25 °C. Prior to CH_3CH_2OD addition, the vesicles were extruded 35 times through 100 nm and then 50 nm pore-sized membranes. Points with errors represent measured data while lines represent fits obtained with a Multilayer Vesicle model. Data are plotted on a log-log scale.

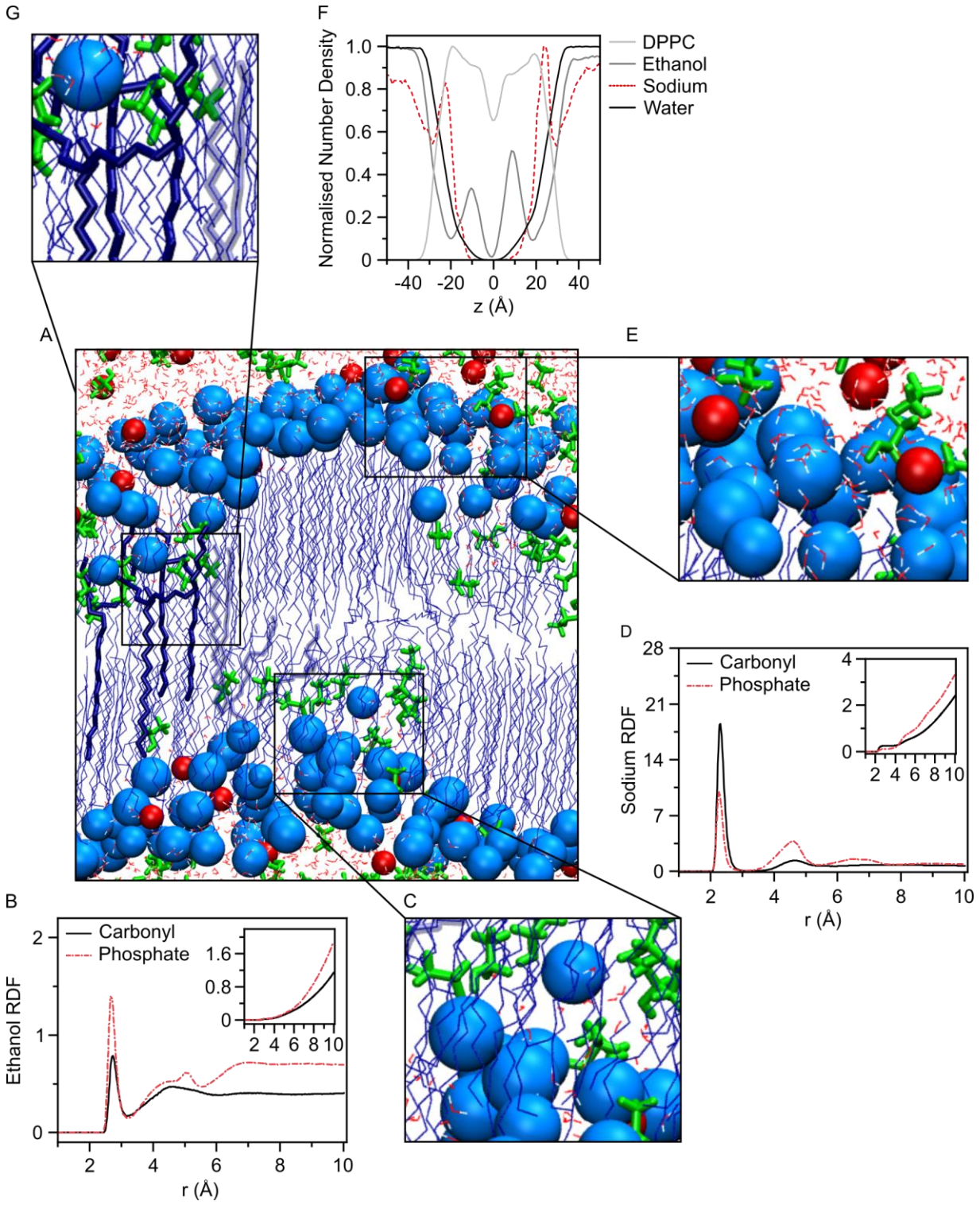

Figure S5. (A) Pictorial representation of the DPPC lipid bilayer in the presence of an aqueous solution of 0.6 M NaCl and 4 M ethanol after 600 ns MD simulations. The sodium ions and the ethanol molecules are depicted in red beads and green bars, respectively, while the water molecules are depicted in red lines. The lipid headgroup area is represented by light blue beads and the lipid chains are represented by dark blue lines. Lipid chains from the upper leaflet have been coloured in a lighter blue for clarity. (B) RDF for ethanol coordination with the carbonyl (black solid line) and phosphate (red dashed line) oxygens of DPPC and (C) zoom-in of the interactions between the lipid

headgroups and ethanol molecules. (D) RDF for Na^+ coordination with the carbonyl and phosphate oxygens of DPPC and (E) zoom-in of the interactions between the lipid headgroups and the sodium ions. In both cases, the cumulative curves of the RDFs are shown as insets. (F) Normalised number densities of DPPC (light grey), ethanol (grey), sodium ions (red, dotted) and water (black) across the bilayer. (G) Zoom-in showing lipid chains and ethanol molecules within the bilayer.

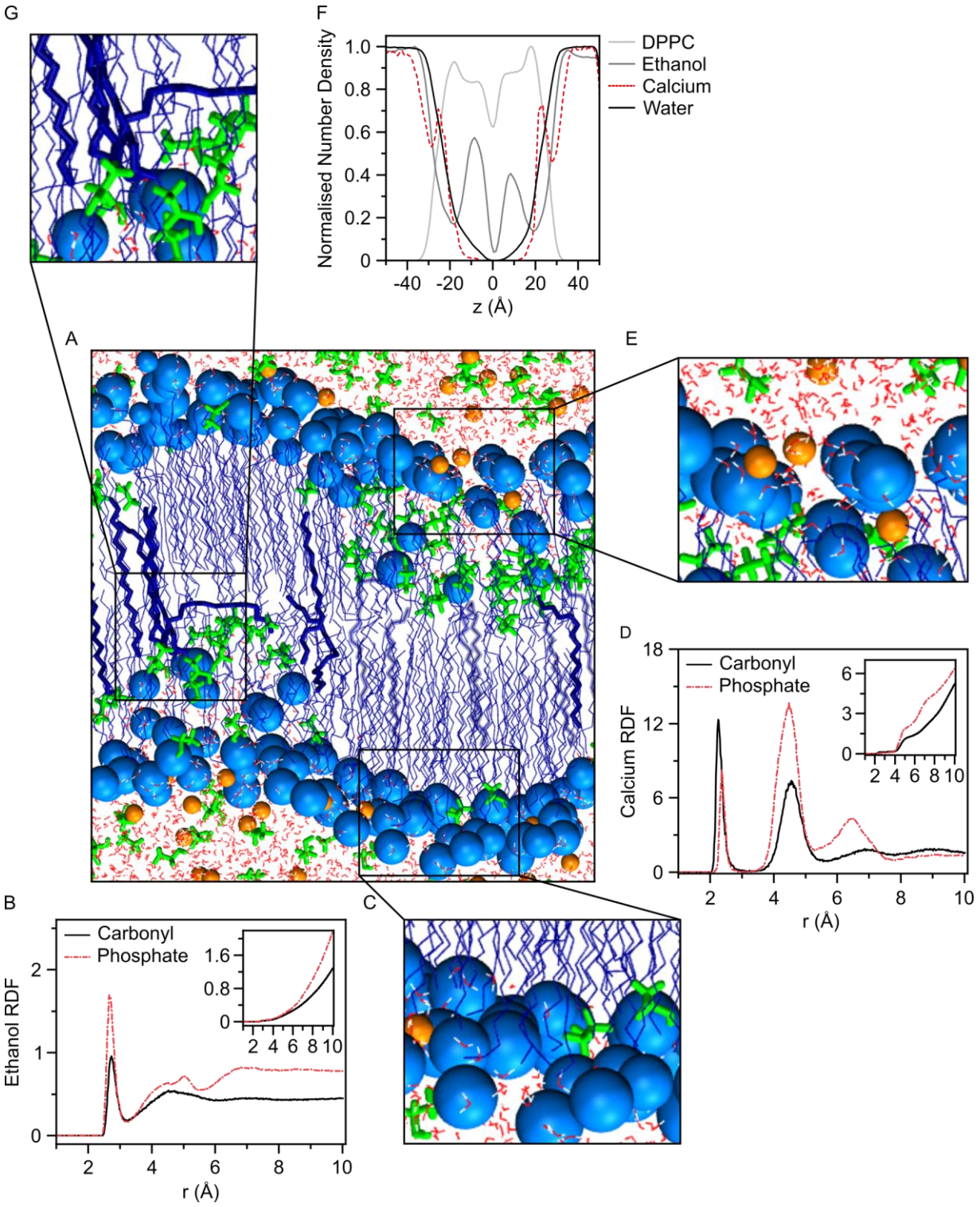

Figure S6. (A) Pictorial representation of the DPPC lipid bilayer in the presence of an aqueous solution of 0.6 M $CaCl_2$ and 4 M ethanol after 600 ns MD simulations. The calcium ions and the ethanol molecules are depicted in orange beads and green bars, respectively, while the water molecules are depicted in red lines. The lipid headgroup area is represented by light blue beads and the lipid chains are represented in dark blue lines. Lipid chains from the bottom leaflet have been coloured in a lighter blue for clarity. (B) RDF for ethanol coordination with the carbonyl (black solid line) and phosphate (red dashed line) oxygens of DPPC and (C) zoom-in of the interactions between

the lipid headgroups and ethanol molecules. (D) RDF for Ca^{2+} coordination with the carbonyl and phosphate oxygens of DPPC and (E) zoom-in of the interactions between the lipid headgroups and the calcium ions. In both cases, the cumulative curves of the RDFs are shown as insets. (F) Normalised number densities of DPPC (light grey), ethanol (grey), calcium ions (red, dotted) and water (black) across the bilayer. (G) Zoom-in of the lipid chains in the bilayer.

References

1. Förster, S. *et al.* Scattering Curves of Ordered Mesoscopic Materials. *J. Phys. Chem. B* **109**, 1347–1360 (2005).
2. Hammouda, B. A new Guinier–Porod model. *J. Appl. Crystallogr.* **43**, 716–719 (2010).